Replies (*in italics*) to the following comments of Reviewers 2 and 3

Anonymous Referee #2

General comments

This article presents the results of a validation study for the Nimbus 7 / LIMS HNO3 and NO2 v6 data sets. The study focuses on the Aleutian High region, in January 1979, when occurred a minor stratospheric warming event. An earlier analysis showed that, in the previous version of these data sets, the evolution of NO2 mixing ratios was inconsistent with the evolution of HNO3 mixing ratios, at this particular time and place. The authors have re-investigated this event using the v6 dataset, together with photochemical calculations, and showed that the data quality has improved. This paper presents interesting and novel results, showing that the v6 LIMS observations can be used for scientific studies. This is perfectly suited to the scope of AMT and I recommend publication after consideration of the minor revisions suggested below.

Given that the main goal of your study is to show that v6 HNO3 and NO2 LIMS data products are of better quality than v5 data products, why do not you show any direct comparison of these two versions? Rather than comparing them only indirectly by referring to the findings of R93, you could for example add at least one figure and one paragraph addressing the direct comparison of these two datasets in the specific region and time period considered in your study. This is true especially for NO2, that has changed the most. This would add value to your paper.

We regenerated Figure 4 (see below) which shows results for both V5 and V6 at 64°N, since the V5 data are not available at 66°N; V5 profiles are at 4° latitude intervals, rather than every 2° as for V6. The primary changes are for NO2, where the V6 values are about half those of V5. Remsberg et al. (JGR, 1994) describes the effect of improved spectral line data for the retrieval of V6 NO2 and we add that reference to the list.

I think that the general readability of the paper could be improved. Some parts of the text consist of a long description of the figures, but your conclusions are not made clear enough. The presentation quality of the figures could also be improved (see specific comments below).

We have rewritten the conclusions slightly to make them clearer.

Specific comments

L69: It would be clearer if you would change ”or the sum of” to something like ”, which is defined as the sum of...”. Moreover N2O5, which is considered in your study, is also part of the NOy family. You could mention it.

We made changes per your suggestion.

L155: Please give more details about how anomalies are defined in your study. Over which period has the zonal mean used as a reference been calculated? In the next paragraph, when writing about the anomalies for NO2, you mention that you took into

account zonal waves also. How have you done exactly? Were the anomalies derived in a different way for different species? Please make that point clearer.

We added more information about the calculation of the zonal anomalies, which are with reference to the daily zonal mean coefficients.

L181: To which pressure level correspond this figure? I guess that it is 31.6 hPa, as in the previous figures. Please mention it, both in the text and in the figure caption.

We now say 31.6 hPa.

L206 and 210: Why do not you represent these uncertainties in the figure? (same comment for Fig. 4)

We added estimates of uncertainty to Figures 4 and 5 and explain them in the text.

L216-224: Please make clearer the link between this discussion on LIMS NO2 L2 products and your figure 5. This paragraph sounds like a general description of the data quality, but it is not clear what is your conclusion and how this affects the interpretation of Fig. 5.

The data in Figure 5 are from the LIMS V6 Level 2 profiles, while the zonal variations in Figure 4 are at grid point longitudes based on the Level 3 Fourier coefficient data.

L236: ”09Z on 28 January” Please explain what is this time format.

Time is 9 am GMT (designated 09Z within most atmospheric datasets) on 28 January.

L258: ”only a modest amount of aerosol surface area is necessary ...” Please quantify this statement.

Aerosol surface area in the model is ~4 x (10-9) per cm at 31 mb and 60N for January. This is equivalent to the value given in Table 1 of Hofmann and Solomon (JGR, 1989) for a background aerosol layer at 25 km, 28N. We've added that reference.

L263: ”an updated version of the stratospheric diurnal photochemical model” Could you briefly explain what are the differences between this version of the model and the version described in Natarajan and Callis (1997).

Reaction rates and photochemical rates in the model are now according to Burkholder et al. (2015).

L300 and 304: Maybe you could add the temporal evolution of the air parcel latitude to your plot. It would thus be easier to follow the interpretation. (same comment for Fig. 9)

We elected not to include information about physical location in the Figures 8 and 9.

L454: The highest value of HNO3 is 13 ppbv, according to Fig. 13.

We revised the upper limit value.

L481-500: I am not convinced that it is useful to separate the description of what happened at high and middle equivalent latitudes into two paragraphs. It makes your text a bit repetitive. (For example, what you wrote in lines 498 to 500 sounds redundant with what you wrote in lines 486-487.)

We moved sentences at lines 496-500 to the end of the previous paragraph.

Fig. 4: Please indicate in the caption the concentration unit for each species (ppmv or ppbv), like you have done for Fig. 8.
Fig. 5: Same comment as for Fig. 4.

We made changes to both figure captions.

Fig. 7: It would be good to find a way to better distinguish the trajectories from each other. (As it is now, it is quite difficult to distinguish the trajectory A-a from B-b.) Maybe adding thin black contour lines could help.

We modified Fig. 7, showing A-a with a thin white center line in (a) and a thin black line in (b).

Fig. 8: You could add the names of the species in the beginning of the corresponding lines. This would make the figure clearer (same comment for Fig. 9). You should also define the red solid line in the caption, as it has been done for Fig. 9.

Species names are at the left of each curve, and we describe the red curves in the captions.

Technical corrections
L29: 27 January (instead of 28).

28 January is correct.

L86: Please remove the second ”unscreened”.
L276: ”that have behavior similar to” Please reword (”that have a similar behavior to...” or ”that behave similarly...” for example).
L401: ”aerosol, surface area” Please remove the comma.
L470: Please change ”during sunlight” to ”under sunlit conditions”.
L711: ”gas phase nitric” The word ”acid” is missing.

We made corrections.

L740: Please change ”between 21 and 27 January” to ”on 21 and 27 January”.

We revised the sentence in the caption to say, 'Note that between 21 and 27 January, there is some repetition of the AH center location and the corresponding red squares overlap'.

Fig. 12: Please write the years in white instead of black.

We made that change. At line 444 we now refer to Colucci and Ehrmann (JAS, 2018), as well.

Replies (*in italics*) to Reviewer 3:

The paper "On the consistency of HNO3 and NO2 in the Aleutian High Region from Nimbus 7 LIMS Version 6 dataset" uses data from the LIMS instrument in January 1979 together with results from a photochemical trajectory model to investigate an event of HNO3 increase in the warm part of a dominant wave-2 structure in the lower stratosphere (30 hPa). Two aspects of this investigation are of interest: 1) The study demonstrates that LIMS v6 observations of HNO3, NO2, temperature and ozone can be used for scientific studies. Though the measurement period of LIMS was relatively short (October 1978 to May 1979), to my knowledge no other global observations of HNO3, or NO2/ozone during night, were available at that time. 2) A dedicated photochemical model study of the role of heterogeneous chemistry in a relatively warm winter stratosphere is carried out, an area certainly not as well investigated as the cold stratospheric vortex; it is found that even in the warm winter stratosphere, heterogeneous chemistry on the background aerosol plays a significant role in re-distributing NOy during night. The paper is reasonably well written, and I recommend publication with a few minor revisions. Some suggestions, mostly related to readability of the text and figures, are listed below.

line 69: ... that includes the chemistry of reactive nitrogen (NOy), the sum of HNO3 and odd nitrogen (NOx) (comma instead of or?)

Line 69: We added a comma.

line 73: here as well as in other places where a zonal wave-2 signature in HNO3 is discussed: I would rather call this a "quasi-wave 2 signature", because it is likely not related to a real planetary (Rossby) wave structure, as you indeed show in the paper. You could also say that it shows a quadrupolar structure. E.g., line 76; line 171; line 382.

Line 73: We changed the terminology, where appropriate.

line 76: "independent of dynamics" but heterogeneous reactions are temperature dependent, and transport plays a role as well here. Maybe it would be better to characterize the behavior of HNO3 as driven by a combination of chemistry and dynamics.

Line 76: We agree that your description is better so we made a change.

line 86: two "unscreened" in this sentence, one of them is unnecessary.

Line 86: We made a correction.

line 137, figure: observed HNO3 is highest in the polar vortex, and particularly in the presence of PSCs. However, as HNO3 is taken up into PSCs, a decrease of gas-phase HNO3 might also be expected in the presence of (large) PSCs (von Koenig et al., JGR, 2002; Lambert et al., Atmos Chem Phys, 2008)

Line 137: We agree with your assessment that it is likely that there was a decrease of gas-phase HNO3 directly downwind of the observed PSCs. We have modified this sentence, accordingly, and have included your two references. However, we believe that Lambert et al. has a publication year of 2012.

line 172-173: Please provide more detail about the derivation of the anomalies. Did you fit zonal planetary wave signatures as well as subtract the zonal mean? How? Why?

Lines 172-173: The zonal anomalies in Figures 2 and 3 are a result of merely subtracting the zonal mean coefficients (or mixing ratio) from the total value at each latitude/longitude grid point. However, the so-called "zonal anomalies" for NO2 represent the result of subtracting the average of the descending or "11 pm" value at a latitude from the total values of NO2 at each longitude. In other words, the separate analyses of the ascending or descending NO2 in the LIMS Level 3 product do not account for likely diurnal variations in the NO2.

line 177: "... while HNO3 and NO2 have anomaly patterns of the same sign" on January 19, but not on January 27 in the Ah region.

Line 177: We agree that the HNO3/NO2 anomalies are of the same sign across the AH region on 17 January but not on 27 January, and we now make that distinction in the revised text.

lines 181-196, figure 4: it would be good to provide error bars in the figure, and discuss the error range of the observations in the text, to assess whether the observed zonal variation is significant. This is especially true for NO2, where variations are small. Error ranges are provided in the discussion of figure 5, but should be provided here as well.
line 188: are "observed? seen?"

Lines 181-196 and Figure 4: The zonal variations in revised Figure 4 (see below) are species values at 64°N, as obtained from the Level 3 Fourier coefficients for both V6 and V5 and calculated at grid points spaced every 5.625° of longitude. The LIMS Fourier coefficients for each of the species are the result of applying a sequential estimation algorithm to their Level 2 or profile data, as limited by the estimated data precisions. As a result, the species variations in Figure 4 are relatively accurate and significant, at least to the scale of zonal wave 6 (or to wave

4 for NO2). The error bars in revised Figure 4 are the $2\sigma_n$ values from the error covariance matrix of the vector of the V6 Fourier coefficients (Remsberg and Lingenfelser, 2010).

Line 188 will say that the "differences for NO2 are seen mainly in the longitude sector from 320 to 120 E."

figure 5: it would be good to provide error bars in figures 4 and 5. I admit figure 5 is quite busy already; however, lines could also be highlighted by color, or you could provide one error range for every species at the edge of the figure. As is it at the moment, it is difficult to asses whether the temporal evolutions of ozone, water vapor and NO2 are significant.

Figure 5: The species variations with time shown in Figure 5 are taken from the orbital or Level 2 profiles nearest to the center of the AH on each day, and we now include estimates of their single profile error. Vertical bars based on those root-sum-squared (RSS) data errors are on each curve near the right hand side of revised Figure 5 (see below).

lines 263-264: please specify in which way the model is updated - reaction rates, heterogeneous chemistry?

Lines 263-264: We use an updated version of the stratospheric diurnal photochemical model (Natarajan and Callis, 1997) that incorporates the chemical kinetics and photochemical data from the recent JPL evaluation (Burkholder et al., 2015) to calculate the changes in the composition of the air parcels until they reach the AH region on 27 January.

line 276: "have behavior" –> "behave"

Line 276: We made the change.

line 458: "when further chemical changes are inefficient" however, there should be uptake into PSCs if cold enough.

Line 458: We are adding your modifying statement.

line 476: "values_7ppm" –> "values of _7 ppm"

Line 476: We made the change.

figure 11: is the scatter within the single profile error of LIMS?

Figure 11: The RSS error estimates for HNO_3 and NO_2 are 0.8 ppbv and 0.24 ppmv, respectively.

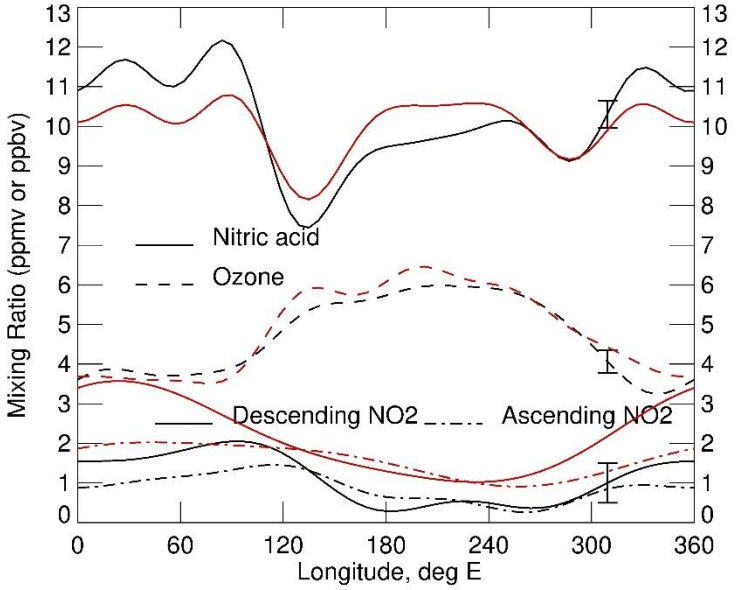

Revised Figure 4 with 2σ error estimates on the V6 curves near 311°E. The data are from the V6 (black) and V5 (red) Level 3 or Fourier coefficient files for January 27, 1979.

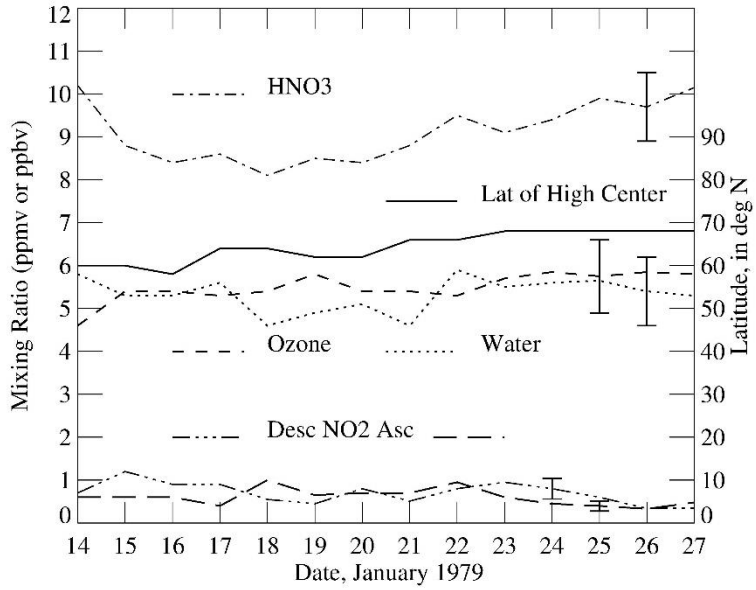

Revised Figure 5 that includes ±RSS errors at January 24-26 for variations of V6 species.

ON THE CONSISTENCY OF HNO_3 AND NO_2 IN THE ALEUTIAN HIGH REGION FROM THE NIMBUS 7 LIMS VERSION 6 DATASET

Ellis Remsberg[1], Murali Natarajan[1], and V. Lynn Harvey[2]

[1]Science Directorate, NASA Langley Research Center

21 Langley Blvd, Mail Stop 401B

Hampton, Virginia 23681, USA

[2] Laboratory for Atmospheric and Space Physics

Atmospheric and Oceanic Sciences

University of Colorado, UCB 311

Boulder, Colorado, 80309, USA

Correspondence to: Ellis Remsberg (ellis.e.remsberg@nasa.gov)

Formatted: Left

Formatted: Normal

Abstract. This study uses photochemical calculations along kinematic trajectories in conjunction with Limb Infrared Monitor of the Stratosphere (LIMS) observations to examine the changes in HNO_3 and NO_2 near 30 hPa in the region of the Aleutian High (AH) during the minor warming event of January 1979. An earlier analysis of Version 5 (V5) LIMS data indicated increases in HNO_3 without a corresponding decrease in NO_2 in that region and a quasi-wave- 2 signature in the zonal distribution of HNO_3, unlike the wave- 1 signal in ozone and other tracers. Version 6 (V6) LIMS also shows an increase of HNO_3 in that region, but NO_2 is smaller than from V5. The focus here is to convey that ~~both~~ V6 HNO_3 and NO_2 are of ~~better~~good quality ~~than from V5~~, as shown ~~here~~ by a re-examination of their mutual changes in the AH region. Photochemical model calculations initialized with LIMS V6 data show increases of about 2 ppbv in HNO_3 over 10 days along trajectories terminating in the AH region on 28 January. Those increases are mainly a result of the nighttime heterogeneous conversion of N_2O_5 on background stratospheric sulfuric acid aerosols. Changes in the composition of the air parcels depend on the extent of exposure to sunlight and, hence, on the dynamically controlled history of the trajectories. Trajectories that begin in low latitudes and traverse to across the Pole in a short time lead to the low HNO_3 in the region separating the anticyclone from the polar vortex, both of which contain higher HNO_3. These findings help to explain the observed seasonal evolution and areal extent of both species. V6 HNO_3 and NO_2 are suitable, within their errors, for the validation of stratospheric chemistry/climate models.

Formatted: Font: 11 pt

Formatted: Font: 11 pt

Formatted: Font: 11 pt

Formatted: Font: 11 pt

Formatted: Font: 11 pt

Formatted: Left

Formatted: Normal

1 Introduction and Objectives

The Limb Infrared Monitor of the Stratosphere (LIMS) experiment operated on Nimbus 7 from 25 October 1978 through 28 May 1979. LIMS measurements were originally processed and archived to a Version 5 (V5) data set (see Gille and Russell, 1984, and references therein). Since then, the observed LIMS radiance profiles have been re-processed with improved, Version 6 (V6) algorithms to provide profiles of temperature, chemical species, and geopotential height, as a function of pressure-altitude from 65˚ S to 84˚ N latitude (Remsberg et al., 2004). There are improvements from the registration of the LIMS radiance profiles and from updated spectroscopic line parameters for retrievals of the V6 species profiles. Several studies already show that the V6 ozone is of better quality for scientific analysis (Natarajan et al., 2002; Stolarski et al., 2013; Remsberg et al., 2013; Shepherd et al., 2014). The two nitrogen species, nitric acid (HNO_3) and nitrogen dioxide (NO_2), are also of better quality ~~in V6,~~ particularly NO_2 (Remsberg et al., 2010~~). In particular,~~; Remsberg et al., 1994). Holt et al. (2012) ~~were able to quantify~~quantified the exchange of V6 NO_2 from the mesosphere to the middle stratosphere within the polar vortex. Remsberg and Harvey (2016) also found good relationships on the 550 K potential temperature surface (near 30 hPa) for the highest values of V6 HNO_3, lowest values of ozone, and highest values of potential vorticity (PV) within the Arctic winter vortex. While there are residual effects from polar stratospheric clouds (PSCs) in the ozone and water vapor (H_2O), those effects are small in the HNO_3 and NO_2 profiles and occur only at temperatures < 194 K and from about 1-20 January. The V6 data set is part of the SPARC Data Initiative for chemistry-climate model comparison studies (Tegtmeier, et al., 2013; SPARC, 2017).

~~The northern~~Northern hemisphere (NH) polar winter of 1978-1979 was dynamically active in the middle stratosphere, as determined from daily surface plots of geopotential height (GPH), potential vorticity (PV), and ozone on the 850 K potential temperature surface (near 10 hPa) (McIntyre and Palmer, 1983;

Formatted: Space After: 8 pt

Formatted: Left

Formatted: Normal

Leovy et al., 1985; Butchart and Remsberg, 1986). A major, zonal wave- 1 forcing brought about a rapid exchange of air between polar and middle latitudes from mid to late January. Rood et al. (1993) (hereafter referred to as R93) analyzed the LIMS V5 data in the Aleutian High (~~hereafter referred to as~~or AH) region for 14-27 January. They reported that the tracer-like species HNO_3 on the 30-hPa surface increased slowly during that time in the region of the relatively warm anticyclone. The absence in their analysis of a corresponding decrease in NO_2 accompanying the increase in HNO_3 led to concerns of an inconsistency in the LIMS data. The present study reconsiders that anomaly but using the V6 dataset and a trajectory model that includes the chemistry of reactive nitrogen (NO_y~~)~~), or the sum of NO, NO_2, $2N_2O_5$, NO_3, HNO_3, HO_2NO_2, and ~~odd nitrogen (NO_x)~~;$ClONO_2$.

In their analysis of the V5 data, R93 also noted finding high values of HNO_3 in both the polar vortex and the AH, and lower values around the periphery of both circulation systems resulting in a ~~zonal~~ quasi-wave- 2 signature in the HNO_3 distribution. They suggested that, since dynamically controlled species like ozone showed a clear wave-1 signature similar to GPH and PV, the HNO_3 levels outside the polar vortex may have influences from a ~~mechanism independent~~combination of chemistry and dynamics in order to account for its quasi-wave- 2 variation. They explored the possible role of heterogeneous chemistry on background sulfate aerosols in converting NO_x to HNO_3 and concluded based on a 2-D model study that those species changes from V5 are large in winter but not correct phenomenologically. Separate studies have shown that heterogeneous reactions involving sulfate aerosols do perturb the stratospheric photochemistry and HNO_3 levels (Austin et al., 1986; Rodriguez et al., 1991). With the availability of the improved V6 dataset, we revisit the question of inconsistency for the LIMS HNO_3 and NO_2 observations in the AH region. We focus our attention on the same period, namely 14 – 27 January, when there was a minor stratospheric warming.

Formatted: Font: Calibri

Formatted: Left

Formatted: Normal

Section 2 describes briefly the improvements implemented in the retrievals of the V6 profiles. We also note that the ~~unscreened,~~ residual effects from unscreened PSCs in the polar vortex are small for HNO_3 relative to those in ozone. Section 3 contains polar plots of ozone, HNO_3, NO_2, and GPH for 17 and 27 January 1979 and describes their changes, as the AH develops and the center of the vortex moves off the Pole. Section 4 shows the changes in V6 HNO_3 and NO_2 at the center of the AH from 14 to 27 January. Section 5 describes an ensemble of trajectory calculations, including heterogeneous chemistry, for air parcels converging in the region of the AH on 27 January. Those calculations partition NO_y into the observed HNO_3 and NO_2, plus the unobserved variations of nitric oxide (NO) and nitrogen pentoxide (N_2O_5). The calculated daily species values compare reasonably well with closest observed LIMS values, as shown from the results in Section 6. We then show in Section 7 time series of variations of PV and of V6 HNO_3, H_2O, and NO_2 on the 550 K potential temperature surface across most of the northern hemisphere for the entire 7¼ months of LIMS data. In this way, the variations for January are set in the context of the longer-term, seasonal changes for those species. Section 8 is a summary of the findings.

2 Improvements of the LIMS V6 species

The LIMS instrument obtained profiles of atmospheric limb radiance in six channels, a wide (W) and a narrow (N) band channel for CO_2 (CO_2W and CO_2N) and one each for ozone, H_2O, HNO_3, and NO_2 (Gille and Russell, 1984). Retrieved V6 profiles occur at a spacing of every 1.4° of latitude (~155 km) along the orbit, although their horizontal, tangent-path resolution remains no better than about 320 km. Bandpass filters (in cm^{-1}) for the LIMS instrument are CO_2W (579-755), CO_2N (637-673), ozone (926-1141), H_2O (1370-1560), HNO_3 (844-917), and NO_2 (1560-1630) in terms of their 5 % relative response points. Both the H_2O and NO_2 channels have an instantaneous field-of-view (IFOV) vertical width at the horizon of 3.6 km, while the other four channels have half that width or 1.8 km.

Formatted: Left

Formatted: Normal

Retrievals of the V6 temperature and associated species profiles were obtained by using all successive, up/down scan profile pairs along their observed, orbital tangent-path locations and at 18 levels per decade of pressure-altitude, p(z), or spaced about every 0.88 km. The effective vertical resolution is the same (~3.7 km) for the retrieved V6 temperature and for each of the species profiles (Remsberg et al., 2004), such that one can evaluate better the combined changes of HNO_3 and NO_2 at a given pressure-level. Further, the spectral line parameters used for the retrieval of the NO_2 were updated for the production of V6, leading to values of nighttime NO_2 that are up to 20 % smaller than those of V5 in the upper and middle stratosphere (e.g., Remsberg et al., ~~2010~~1994). An important addition to the V6 data set is the co-located GPH for each of the retrieved profiles.

LIMS-retrieved ozone has a non-linear sensitivity to temperature and/or radiance biases and to the effects of PSCs; retrieved H_2O mixing ratio is even more sensitive (Remsberg et al., 2007; 2009). On the other hand, effects from PSCs are much less noticeable in HNO_3 and NO_2. As an example, Figure 1 shows the relative effects for ozone and HNO_3 of the residual contamination or the unscreened effects of emission from PSCs, plus the associated temperature and GPH on the 31.6-hPa surface for 11 January. Grid-point data for the surface plots of Fig. 1 are from the V6 Level 3 sequential estimation (SE) algorithm product (Remsberg and Lingenfelser, 2010). The ozone panel of Fig. 1 shows values in the cold vortex region that are of the order of 6 ppmv and not in keeping with the much lower surrounding values of 3 ppmv. White plus signs indicate where there was a screening of profile segments perturbed by emissions from PSCs in ozone, and the red dot indicates the presence of a PSC based on data from the Stratospheric Aerosol Monitor (SAM II) experiment for comparison purposes. While there can be descent of ozone in the vortex from higher altitudes, the excess ozone in the vortex region of Fig. 1 is due to the remaining, unscreened effects of the PSCs. Note also that the PSC features occur only where the environmental

Formatted: Left

Formatted: Normal

temperature is less than about 194 K. Thus, effects of PSCs are minimal for most of the Arctic lower stratosphere, and they are not present at all in the warmer AH region.

The lower right panel of Fig. 1 shows that observed HNO_3 ~~also has values~~is highest in the vortex ~~that appear a bit high.~~, and particularly in the presence of PSCs. As HNO_3 adsorbs onto PSCs, a decrease of gas-phase HNO_3 is also expected in the presence of and directly downwind of large PSCs (von Koenig et al., 2002; Lambert et al., 2012). Yet, those high LIMS values are nearly unaffected by ~~the~~ PSCs because the relationship between the ~~observed~~ LIMS HNO_3 channel radiance and its retrieved mixing ratio is ~~very nearly~~essentially linear. In fact, simulation studies indicate that a temperature bias error of 1 K has only a small, 3 % effect in the V6 HNO_3 mixing ratios from 10 to 50 hPa (Remsberg et al., 2010, their Table 1). Retrieved NO_2 also varies in a nearly linear way. Yet as with ozone, there are no perturbing effects from PSCs for H_2O, HNO_3, or NO_2 in the AH region that is the focus of the remainder of this study.

3 LIMS V6 GPH, O_3, HNO_3, and NO_2 during January 1979

R93 (and references therein) analyzed and presented results of GPH, ozone, and HNO_3 at 30 hPa from the V5 data set for 14, 17, 23, and 27 January. They noted that ozone behaves as a tracer in terms of its relation to changes in GPH and according to its associated transport fields. On the other hand, they found that the HNO_3 distributions did not evolve in the same way, but developed a ~~zonal~~ quasi-wave- 2 rather than wave- 1 character over a deep layer of the middle stratosphere (50 to 5 hPa). They also did not find clear anti-correlations between the distributions of V5 HNO_3 and NO_2 in the more isolated AH region, at least to the extent that the sum of those two gases do not change appreciably. We consider their variations again using the V6 data.

Formatted: Left

Formatted: Normal

Initially, Rood et al. (1987) ~~had~~ expressed some ~~doubts~~doubt about the accuracy of the Arctic GPH fields at 30 hPa from the operational meteorological analyses for January 1979. Figs. 2b and 3b are polar plots of the zonal GPH anomalies ~~(deviations from zonal mean) from V6~~ for the equivalent level of 31.6 hPa and for two of the four days above, 17 and 27 January. Those GPH anomalies exhibit structures that are very similar to those ~~of~~found by R93 (their Figs. 1b and 1d). ~~The large~~Large-scale flow is along ~~the~~ isolines of the GPH anomalies or around the respective high and low centers. The AH strengthened significantly but remained at about the same location from 17-27 January.

Anomalies for the LIMS species in Figs. 2 and 3 are a result of subtracting the V6 zonal mean coefficient (or mixing ratio) from the observed values at each latitude/longitude grid point. However, the so-called "zonal anomalies" for ascending (local 1 pm) and descending (local 11 pm) NO_2 represent the result of subtracting the average of the ascending or descending values for a latitude from the corresponding, observed values of NO_2 at each longitude. In other words, the separate analyses of the ascending or descending NO_2 in the LIMS Level 3 product do not account for likely diurnal variations in the NO_2. Maximum ozone anomalies in Figs. 2a and 3a are nearly coincident with the center of the AH, again in close agreement with the findings of R93 (their Figs. 2b and 2d). There is strong meridional transport of air of relatively poor ozone along the western edge of the AH to across the Pole from 17 to 27 January.

~~The large~~Large-scale, zonal anomalies in HNO_3 (Figures 2d and 3d) are opposite in sign to those of GPH and ozone. One exception is the relatively low values of HNO_3 near 80˚ N, 0˚ E on 17 January in Fig. 2d, which has been interpreted as due to an uptake of gas phase HNO_3 onto PSC particles just upwind a day or so earlier (Remsberg and Harvey, 2016). Yet, by 27 January (Fig. 3d) the cyclonic circulation about the low GPH center indicates clearly that there ~~is~~must be net transport of low values of HNO_3 near 140˚ E, along the axis of the polar night jet, across the Pole, and then to about 300˚ E. As a result, while both

Formatted: Left

Formatted: Normal

ozone and NO_2 display the same ~~zonal~~ wave- 1 structures as the GPH field on 27 January, the HNO_3 distribution exhibits quasi-wave- 2 structure. Figs. 2c and 3c represent NO_2 anomalies from profiles of just the LIMS V6 descending orbits, or from its nighttime values near 11~~:00~~ pm local time. Those anomalies for NO_2 are from four zonal waves minus the zonal mean coefficient, rather than from six zonal waves as for all the other LIMS Level 3 products. Most of the NO_x converts from NO to NO_2 at sunset, followed by a further, partial conversion of the NO_2 to N_2O_5 up to the 11~~:00~~ pm observation time of LIMS (Brasseur and Solomon, 2005). The respective panels of Figs. 2 and 3 demonstrate that ozone and NO_2 have large-scale features of opposite sign in the AH region, while HNO_3 and NO_2 have anomaly patterns of the same sign- on 17 January but not on 27 January. Clearly, it is important to consider the amount of NO_x that is in the form N_2O_5 in the AH region during that time span.

Figure 4 shows the zonal species variations from the V6 SE or Fourier coefficients at 31.6 hPa for 27 January at the latitude of ~~66°~~64° N ~~on 27 January,~~ and ~~they~~as calculated at grid points spaced every 5.625° of longitude. The LIMS Fourier coefficients for each of the species are ~~accurate~~ the result of applying the SE algorithm to ~~within the~~ their Level 2 or profile data, as limited by the estimated data precisions ~~for each given species.~~ . As a result, the V6 species variations (black curves) are relatively accurate and significant, at least to the scale of zonal wave 6 (or to wave 4 for NO_2). Vertical error bars in Fig. 4 are the 2σ values from the error covariance matrix of the vector of the V6 Fourier coefficients (Remsberg and Lingenfelser, 2010). Variations from the V5 data set at 30 hPa are included for comparison purposes (red curves).

HNO_3 within the polar vortex (0° to 90° E) is higher by nearly 2 ppbv compared to that in the AH region (180° E to 240° E). Note from Fig. 3, however, that HNO_3 has a strong, positive Equator-to-Pole gradient in the 0° to 90° E sector, whereas that of ozone is weak and slightly negative. Ozone in Fig. 4 has a

Formatted: Left

Formatted: Normal

broad, wave- 1 character, while HNO_3 exhibits two minima (at ~~140~~130° E and ~~300~~290° E). At 10 hPa and lower pressures (or at higher z) a quasi-wave- 2 structure is no longer apparent in HNO_3. Variations of the descending and ascending (daytime or ~~1330~~1:30 pm local time) NO_2 modes appear separately in Fig. 4. Diurnal differences for NO_2 are seen only in the longitude sector from ~~60~~320°E to 120˚ E, or across the boundary of the cold polar vortex and the warmer AH region. Relatively low ozone ~~at~~in this ~~location~~region results in only a slow conversion of NO_2 at sunset to NO_3 and finally to N_2O_5. Consequently, a larger fraction of NO_x remains as NO_2 at the time of the LIMS descending mode observations, or ~~near~~ ~11~~:00~~ pm local time. The warmer AH region from ~~180~~150° E to ~~240~~270° E, on the other hand, has higher ozone mixing ratio, and the decrease in NO_2 from its maximum at sunset is steeper, bringing NO_2 mixing ratios at the time of the LIMS descending mode observation close to the value of the ascending mode measurement. There is very little diurnal difference in NO_2 in that longitude region. Thus, air parcel history is important for interpreting observed changes in the distributions of these two reactive species even in the AH region.

V5 NO_2 varies in a similar way, although its values are nearly twice those of V6.

4 Changing composition within the Aleutian High

~~Figure 5 shows~~Species variations with time are shown in ~~the V6 species~~Figure 5, as determined from the V6 orbital or Level 2 profiles at 31.6 hPa and ~~at~~nearest to the center of the AH~~, which is~~ on each day and identified by the location of the maximum GPH anomaly. Note that Fig. 5, which is analogous to Figure 7 of R93, also shows that the latitude of the AH moves poleward from about 60° N to 68˚ N from 14 to 27 January. Its longitude moves slightly, too, from 186˚ E on 14 January to 230˚ E on 19 January and then retreats partially to 214˚ E by 27 January. ~~Red boxes in~~ Figure 6 ~~illustrate~~illustrates those locations~~.~~ better as red boxes for each day. GPH of the 31.6-hPa level at the center of AH grows from 23.0 to 23.8 km during that same time.

Formatted: Left

Formatted: Normal

~~Ozone and H_2O variations~~ Vertical bars in Figure 5 ~~are no greater than their estimated single profile,~~represent root-sum-squared (RSS~~) bias~~), single profile errors ~~of ~15 % at~~for 30 hPa (Remsberg et al., 2007; 2009~~). They~~), and the ozone and H_2O variations are no greater than those error estimates of 15 %. Those two species remain rather steady in the AH and are in keeping with their small horizontal gradients on the 31.6-hPa surface and their relatively long chemical lifetimes. HNO_3 shows significant ~~change~~changes; it declines from 10 to 8.2 ppbv from 14 to 18 January, but then increases rather steadily again to 10 ppbv by 27 January. Single profile RSS uncertainty for HNO_3 is ~8 % at 30 hPa (Remsberg et al., 2010). Descending (or late evening) NO_2 declines from 1.1 to 0.5 ppbv from 15 to 19 January, increases to about 1.0 ppbv on 23 January, before declining again to 0.4 ppbv on 27 January. Ascending (early afternoon) NO_2 is smaller than descending NO_2 from 14 to 17 January, or when the AH center is at about 60° N. As the AH central latitude shifts northward after 17 January, both the ascending and descending NO_2 exhibit similar values and indicate that the daytime observations are from near to or within the polar night boundary. Generally, the RSS error for single NO_2 profiles is ~30 % at this pressure level, although ~~it may be a bit~~profile registration uncertainties can lead to larger errors across the polar night boundary. ~~In particular,~~ Remsberg et al. (2010, their Fig. 3) ~~show~~showed an altitude-latitude plot of "zonal average NO_2" from only the descending (11~~:00~~ pm) orbital segments of 15 January, when the polar vortex is still nearly circular and centered on the Pole. Its vertical distribution at 60° N declines from 2.5 ppbv at 20 hPa to a local minimum of < 1 ppbv at 35 hPa or about where the associated HNO_3 ~~also~~ has its local maximum. In fact, the V6 retrieval algorithm sets NO_2 to zero, when the forward radiance for the tangent layer approaches the measurement noise for that channel (5.5×10^{-4} w-m^{-2}-sr^{-1}). Thus, the effect of a finite (~3.7 km) vertical resolution is to smooth across that local NO_2 minimum, giving a high bias in its final retrieved value.

Formatted: Left

Formatted: Normal

5 Trajectory model with photochemistry

In this section, we examine the interplay between photochemistry and dynamics during the evolution of HNO_3 and NO_2 in the AH by making use of photochemical calculations along trajectories that terminate in the AH region on 27 January. In these calculations, we use the V6 level 2 profile data to initialize the air parcel composition, which allows a comparison between model results and co-located observations along the trajectory in the AH region. The trajectory model is driven by 3-dimensional meteorological data from MERRA (Rienecker et al., 2011) corresponding to January 1979. This dataset includes 3-hourly information on surface pressure, horizontal wind, vertical pressure velocity, and temperature on a 1.25° longitude by 1.25° latitude grid. A family of 70 back trajectories is generated, with trajectories beginning at 30 hPa from a grid of 2°-latitude by longitude covering a domain defined by 210° E and 218° E longitudes and 60° N and 86° N latitudes. The starting time of the back trajectories is 9 am GMT (or 09Z) on 28 January, which corresponds to a local time of 11~~:00~~ pm on 27 January at 210° E. This is close to the local time of LIMS descending mode observations in this latitude region. The selected region overlaps the AH in the contour plot of V6 GPH anomalies for this day, as shown in Fig. 3b. The model uses a 4th order Runge-Kutta advection scheme to generate 3-dimensional, kinematic back trajectories. We save trajectory parameters required for further calculations on an hourly basis.

Figure 6 shows the back trajectory beginning on 27 January at 214° E, 68° N and 30 hPa. The numbers in black along the trajectory represent the day numbers. Red colored squares with day numbers represent the history of the location of the AH center at 31.6 hPa based on the maximum V6 GPH anomaly. This V6 pressure level is the closest ~~in LIMS data~~Level 2 value to 30 hPa. It is clear that between 22 and 27 January the trajectory and the AH center remain in a region north of 54° N latitude, and the AH region provides an isolated natural chemical laboratory for the constituents to evolve. Prior to 22 January the trajectory and AH center diverge with the trajectory going backwards to latitudes as far south as 27° N.

Formatted: Left

Formatted: Normal

As we will show later, the back trajectory beginning at 214° E and 60° N remains within the AH region or north of 45° N throughout the 10-day period. These differences among the trajectories affect their initial values and the changes in air parcel composition.

~~Time~~We conducted time-dependent photochemical calculations ~~are conducted~~ along the trajectories in the forward direction. Information used in these calculations include the vertical ozone column along the trajectories based on V6 Level 3 ozone data, background sulfate aerosol surface area densities for January 1979 adopted from the IGAC/SPARC CCMI recommendations for Reference Simulation 1 (Eyring et al., 2013), and solar zenith angle corresponding to the local time of day. ~~Note that only a modest amount of aerosol~~Aerosol surface area in the model is ~~necessary~~4 x 10^{-9} cm^{-1} at 31 hPa and 60°N for ~~the heterogeneous mechanisms to occur (e.g., Austin et al., 1986~~January (see Table 1 of Hofmann and Solomon, 1989). The starting location and mixing ratios of measured species are determined by identifying for each trajectory the spatially and temporally closest LIMS descending mode observation between 14 and 17 January. Longitude separation between the trajectory and the V6 data is within 15°, latitude separation within 7.5°, and time of measurement within an hour. We use an updated version of the stratospheric diurnal photochemical model (Natarajan and Callis, 1997~~)~~), incorporating the chemical kinetics and photochemical data from the recent JPL evaluation (Burkholder et al., 2015), to calculate the changes in the composition of the air parcels until they reach the AH region on 27 January. ~~Chemical kinetics data are adopted from the recent JPL evaluation (Burkholder et al., 2015).~~ Results from a time-dependent, 2-dimensional chemistry-transport model (Callis et al., 1997) simulation corresponding to January 1979 provide initialization estimates of other unmeasured HO_x, Cl_x, and NO_x species. The initialization procedure involves repeated diurnal calculations at the fixed starting latitude, altitude, and day. During each diurnal cycle, the mixing ratios of ozone, NO_2, and HNO_3 are set to the observed values at the local time of the LIMS descending mode measurement (Natarajan et al., 2002). Within five diurnal

Formatted: Left

Formatted: Normal

cycles, the short-lived chemical species reach near steady mixing ratios. Then, the photochemical model integration continues along each trajectory until reaching the endpoint of 09Z on 28 January.

6 Results and discussion

We show in this section the results of sample trajectories that ~~have behavior~~behave similar to those of the ensemble and discuss the transformations occurring in the composition of the air parcels over their 10-day transit. All trajectories terminate at 30 hPa but, since we use 3-dimensional kinematic trajectories based on MERRA, there are fluctuations in pressure and altitude as the parcel moves along its trajectory. The length of exposure to daylight also fluctuates and is not the same for all the trajectories. These differences certainly affect the photochemical changes that occur.

Figure 7a shows, on a polar stereographic projection map of the Northern Hemisphere, three different trajectories terminating at a longitude of 214° E. The latitude circles in the figure are 10° apart and poleward of 20° N. The uppercase letters A, B, and C denote the starting location of the trajectories and the lowercase letters a, b, and c mark the endpoints at 60° N, 72° N, and 80° N latitude, respectively. The color scale ranging from 0 to 1 represents the accumulated hours of exposure to darkness along each trajectory expressed as a fraction of the total length of the trajectory in hours. The cumulative fraction of darkness at the endpoint is 0.70, 0.67, and 0.63 for the trajectories A-a, B-b, and C-c, respectively. Fig. 7b shows the same three trajectories but now color-coded to demonstrate the calculated variation of HNO_3. Trajectory A-a starts at 222.1° E and 59.9° N on 17 January with an initial HNO_3 mixing ratio of 9.05 ppbv, adopted from the nearby LIMS observation. Both the starting and termination points for this trajectory are very near the center of the AH as seen in the GPH anomaly contours (Fig. 3b). The mixing ratio of HNO_3 increases to 10.8 ppbv, mostly due to the heterogeneous hydrolysis involving N_2O_5 and sulfate aerosol. This conversion of NO_x predominates while the parcel is in darkness.

Formatted: Left

Formatted: Normal

Figure 8a shows the variation with time of selected chemical constituents as the air parcel moves along trajectory A-a. Shown by the thick broken line at the top of the figure are the segments when the parcel along this trajectory is in darkness. It is clear that HNO_3 increases during extended periods of darkness, which occur more often when the parcel traverses through higher latitudes. This increase in HNO_3 comes at the expense of other reactive nitrogen species as can be seen in the decrease in the mean value and somewhat diminished amplitude of the diurnal variation of NO_2. There is also a dampening of the diurnal variation of N_2O_5 because of limited exposure to sunlight, although its mean value remains higher. The daytime peak mixing ratio of NO is low (not shown). When a trajectory is at lower latitudes (e.g., between 17 and 22 January), all NO_x species display larger diurnal variations with little change in mean value. HNO_3 also shows some diurnal fluctuations due to daytime photolysis followed by production due to heterogeneous chemistry in darkness and with a slight overall increase in mean mixing ratio. After 22 January, the air parcel moves to higher latitudes and experiences extended periods of darkness, leading to the steady increase in HNO_3. Thus, a combination of dynamics, which determines the trajectory that the parcel follows, and both gas-phase and heterogeneous photochemistry explains the higher levels of HNO_3 measured by LIMS near 30 hPa in the AH region on 27 January. Ozone, which has a longer chemical lifetime at this pressure level, shows almost no change. However, we also note that at lower pressures, e.g., at 5 hPa, there is a similar impact of dynamics and photochemistry in the formation of pockets of low ozone mixing ratio within the AH region during winter (Manney et al., 1995; Morris et al., 1998; Harvey et al., 2004). The photochemical time constant for ozone at those pressure levels is short enough that air parcels originating from lower latitudes and containing higher ozone go through a chemical transformation, when confined for an extended period of time within the AH region. This results in a destruction of ozone in reaching photochemical equilibrium under daylight conditions. Conversely, the increase in HNO_3 at 30 hPa is due mainly to the nighttime heterogeneous chemistry.

Formatted: Left

Formatted: Normal

In order to highlight the role of the heterogeneous reactions involving background sulfate aerosols, we have repeated the photochemical calculations along the same trajectories but considering only gas-phase reactions. Fig. 8b shows the mixing ratios in this case for trajectory A-a. HNO_3 decreases from the initial mixing ratio of 9.1 ppbv and settles to a value closer to 8.0 ppbv by 20 January. Because we initialized the parcel using LIMS HNO_3 data, that initial drop is indicative of the imbalance created by removing the source due to heterogeneous conversion. Small diurnal fluctuations are apparent during the passage through lower latitudes because of photolysis, but they are nearly absent when the parcel is in the high latitude region. Without heterogeneous reactions, N_2O_5 remains the primary reservoir of NO_x during the nighttime and reaches its peak values just when the parcel is about to emerge from darkness. The mean mixing ratio of N_2O_5 is about 2 ppbv between 23 and 25 January, when the parcel experiences that extended period of darkness at high latitude. The diurnal cycle for NO_2 exhibits larger amplitudes when using only gas-phase reactions, since the absence of additional production of HNO_3 keeps the NO_x mixing ratio higher. The difference in the mixing ratio of HNO_3 in the AH region between the two simulations shows the impact of heterogeneous reactions in the partitioning of odd nitrogen. While the agreement for HNO_3 between model and the LIMS data of Fig. 5 is good with the inclusion of heterogeneous reactions, the comparison for NO_2 is worse; the model gives mixing ratios that are lower than the measurement. ~~Considine et al. (1992) also reached a similar conclusion in their 2-dimensional model study.~~ But, that is also when the V6 NO_2 in the AH region is near its local minimum of about 0.5 ppbv, and we noted in Section 4 that such small retrieved values are likely to have a ~~slight~~ high bias.

Trajectory B-b, shown in Fig. 7a, starts from 173.3° E and 23° N on 14 January. After spending a few days in the lower latitudes, the air parcel along this trajectory takes a nearly meridional path to the AH region. During the last 5 days the parcel remains confined in the AH region, similar to the parcel along

Formatted: Left

Formatted: Normal

trajectory A-a. The chemical evolution along the trajectory, shown in Fig. 9a, is also similar to that along trajectory A-a displayed in Fig. 8a. Large diurnal variations in NO_2 and N_2O_5 occur during the initial period between 14 and 20 January, when the trajectory is in the lower latitudes. Even HNO_3 displays noticeable variations with an increase during night caused by the heterogeneous conversion of N_2O_5 followed by a decrease due to photolysis during daytime. Amplitudes of the diurnal variations diminish in the high latitude AH region, due to reduced photolytic loss, especially for HNO_3, during the shorter daylight period and at higher zenith angles. The corresponding increase in the nighttime heterogeneous conversion leads to HNO_3 mixing ratios greater than 10 ppbv at the end of the trajectory. Between 22 to 25 January, NO_2 displays a steady diurnal cycle, while N_2O_5 shows a declining peak value. The increase in HNO_3 does not occur with a corresponding decrease in NO_2. During extended periods of darkness, NO_2 decreases to a negligible amount as shown at the end of the trajectory on 27 January. When there are only gas phase reactions, the variation of HNO_3 is as shown by the red line. Again, initialization of the photochemical model uses the V6 data, and the absence of heterogeneous reactions introduces an imbalance leading to the negative tendency in HNO_3.

Trajectory C-c, shown in Fig. 7a, starts from 79.9° E and 27.6° N on 17 January. Until 24 January, this parcel stays south of 40° N and then takes a meridional path directly northward reaching 80° N by 28 January. This is slightly north of the AH but still outside the polar vortex. Fig. 9b shows variations of the species mixing ratios along the trajectory C-c for the simulation with heterogeneous chemistry. ~~The~~ HNO_3 mixing ratio at the beginning of the trajectory (C) is about 7.8 ppbv, and it increases to about 8.7 ppbv at the endpoint (c). ~~The measurements~~Measurements in Fig. 3d indicate a quasi-wave~~-~~ 2 feature in HNO_3 at ~~30~~31.6 hPa, with peak values in the polar vortex region and AH. The minimum in HNO_3 between these two regions is a result of the rapid transit of air parcels from lower latitude along trajectories similar to C-c. The air parcels remain in the low latitudes for a longer time, and photolysis

Formatted: Left

Formatted: Normal

during daylight hours keeps the net change in HNO_3 low. Only later is there a noticeable increase in HNO_3 for the high latitude segment of the trajectory. NO_2 and N_2O_5 display diurnal variations as expected in the middle latitudes. After 21 January, there is a decrease occurring in the peak value of NO_2 at every successive sunset along the trajectory. The corresponding minimum in N_2O_5 shows a small increasing trend especially after 24 January, and this is due to the increasing lifetime against photolysis at winter high latitudes. The parcel is in complete darkness during the last 24 hours, when NO_2 continuously decreases to a very low mixing ratio, N_2O_5 declines slowly, and HNO_3 increases.

~~Calculated~~Figure 10 shows HNO_3 mixing ratios ~~are shown in Figure 10~~calculated on a longitude-latitude grid for the end time of the ensemble of 70 trajectories, corresponding to 09Z on 28 January. The latitudinal variation in HNO_3 between 60° N in the AH region and the Pole clearly shows a dip to lower values near 80° N in the model calculations. This spatial distribution occurs even when heterogeneous reactions are not included. However, calculations with heterogeneous chemistry simulate the magnitude of the LIMS HNO_3 observations better. Combined with the higher HNO_3 values in the polar vortex (not a focus of this paper), the differing trajectories explain the formation of a ~~wave-2-like~~quadrupole structure at 30 hPa seen in the LIMS HNO_3 observations during the minor warming. As reported by R93, this feature is present in the LIMS V5 data also, except that V5 HNO_3 is nearly of the same magnitude in the AH and the polar vortex at 30 hPa on 27 January. For the same conditions, the V6 HNO_3 is larger in the polar vortex than in the AH by about 2 ppbv.

Even though we have shown and discussed the model results for only three of the trajectories, all of which end along 214° E longitude, the results for the entire ensemble provide a consistent picture. ~~A~~Figure 11a is a scatter plot of the calculated HNO_3 along the 70 trajectories versus the spatially and temporally closest LIMS ~~observation is shown in Figure 11a. There is little bias~~observations.

Formatted: Left

Formatted: Normal

Differences between the model and LIMS data are of the order of the RSS error of 0.8 ppbv, except for mixing ratios greater than 10 ppbv where the model values are higher. ~~A~~Figure 11b is a similar scatter plot for NO_2 ~~is displayed in Figure 11b, where~~ ; model values ~~from the model~~ are lower than the V6 observations~~.~~ that have an RSS error of 0.24 ppbv. Deviations from the diagonal dashed line for both HNO_3 and NO_2 could be due to a variety of factors, in addition to bias errors of the data. The criteria we used for selecting the closest observation are coarse, but tightening those criteria reduces the amount of data available for initializing the model and for comparison along the trajectory. While we used the closest LIMS observation to constrain the initialization of the model, other unmeasured species as well as total odd nitrogen are from two-dimensional model output that introduces some uncertainty. We have used the recommended kinetic rate constants, but any uncertainty in key reaction rates could affect the calculated variations in the composition. Another possible source of error is the background stratospheric aerosol,~~,~~ surface area density. We ~~have~~ used the climatology from IGAC/SPARC CCMI database, which is zonally averaged data. There were no major volcanic perturbations in late 1978 and early 1979, so large perturbations from this database are most unlikely. While at the lower latitudes photolysis during the daylight hours is important in limiting the impact of heterogeneous reactions, the aerosol data directly affects that rate of conversion of N_2O_5 to HNO_3. It may be that background aerosols in the vortex at high latitudes are less abundant than prescribed, which could explain the apparent high bias in model HNO_3 in Figure 11a for values greater than 10 ppbv ~~in Figure 11a~~. Although LIMS did not measure N_2O_5, analyses involving ATMOS measurements show clearly the role of N_2O_5 and heterogeneous reactions in the stratospheric odd nitrogen chemistry (Natarajan and Callis, 1991). A more comprehensive study of the changes in atmospheric composition in the AH region using data from more recent satellite experiments is beyond the scope of this study.

7 Seasonal evolution of PV, HNO_3, H_2O, and NO_2

Formatted: Left

Formatted: Normal

Anticyclone features usually develop in the Northern Pacific stratosphere and are present about 60 % of the time during winter (Harvey and Hitchman, 1996; Baldwin and Holton, 1988). Therefore, we place the V6 species variations of 14-27 January into the broader context of their seasonal variations. As before, one can ignore the effects of any remnants from PSCs for the species away from the polar winter vortex. First, Figure 12 is a time series plot of the dynamical tracer, PV, on the isentropic surface of 550 K (near 31.6 hPa) for 25 October 1978 through 28 May 1979.

$$PV = (f + \zeta) / \sigma \quad , \qquad (1)$$

where $f = 2\Omega \sin \varphi$ is the local vertical component of the planetary vorticity on a pressure surface and $\zeta = (r \cos \varphi)^{-1} (\partial v/\partial \lambda - \partial(u \cos \varphi)/\partial \varphi)$ is the relative vorticity in polar coordinates (longitude λ and latitude φ). σ is isentropic density (kg m^{-2} K^{-1}) and $1/\sigma = -g\, \partial\theta/\partial p = (1/\rho)\, \partial\theta/\partial z$ is static stability. Geostrophic wind components, u and v, are calculated at grid points from the V6 GPH fields. Then, daily values of the vertical component of PV are computed at each grid point from the zonal and meridional components of the wind (u and v), plus the local vertical gradients of potential temperature versus pressure from V6, following Harvey et al. (2009). The ordinate of Fig. 12 is in terms of equivalent latitude φ from the Pole (90˚) to 15˚ N and is from a monotonic ordering of the daily PV from high values inside the polar vortex to lower values outside (see e.g., Butchart and Remsberg, 1986). Thus, equivalent latitude is a vortex-centered coordinate that assigns the highest PV values (located in the center of the vortex) to be at 90° N. Tic marks along the abscissa denote the middle of each month, and the PV time series have a seven point smoothing. The ordinate is linear in φ to accentuate variations in the PV field at high equivalent latitudes. The effects of the AH on the displacement and erosion of the PV vortex during 14-27 January are in Fig. 12 from φ of about 60° to 90° and following the tic mark labeled 01 on the abscissa.

Formatted: Left

Formatted: Normal

The effect of the AH in peeling away material contours from the edge of the polar vortex has been described aptly (e.g., McIntyre, 1995; Juckes and McIntyre, 1987; Rose, 1986). Fig. 12 indicates the continual erosion of highest PV values during late winter and early spring due to zonal planetary wave- 1 (the AH) and wave- 2 activity. The adjacent "surf zone" region of lower PV values expands and exhibits weakened gradients ($\varphi \sim 30°$ to 60°) from the meridional mixing of PV across both the lower and higher latitudes (McIntyre and Palmer, 1983). It is also noted that the vortex was split (wave-2) at four separate times at the level of 31.6 hPa: late October, late November/early December, late February, and in early April. Both scales of zonal forcing are indicative of the effects of planetary wave activity as it propagates from the troposphere to the 31.6-hPa level (Juckes and O'Neill, 1988).) and/or of a poleward eddy heat flux (Colucci and Ehrmann, 2018). The meridional gradient of PV is quite weak equatorward of $\varphi \sim 60^{\circ}$ N in winter and then across all latitudes by mid-April, or after the polar vortex has undergone significant erosion. The large-scale anticyclones and associated zonal easterlies expand toward the middle latitudes by April.

The Figure 13 shows the corresponding HNO_3 distribution is shown in Figure 13, as determined by averaging itsHNO_3 values around the daily PV contours and orderedthen ordering them according to the φ of Fig. 12. Those averages represent approximate, modified Lagrangian mean (MLM) values for HNO_3 or its average values around the PV contours, and they enable one to identify differences in behavior (e.g., chemical changes) for trace constituents versus PV (McIntyre, 1980; Butchart and Remsberg, 1986). HNO_3 varies nearly monotonically with latitude at this level, and values as high as 1213 ppbv are found near the center of the vortex ($\varphi = 90^{\circ}$) by late November and during the polar night. Such high values indicate a nearly complete chemical conversion of the available NO_y to its reservoir speciescomponent HNO_3. Poleward of about $\varphi = 70^{\circ}$ the HNO_3 contours are aligned well with those of PV, indicating that HNO_3 is an excellent tracer at 550 K, particularly in winter polar night when further chemical changes are

Formatted: Subscript

Formatted: Left

Formatted: Normal

inefficient. However, there should be some HNO_3 uptake into PSCs, when temperatures become cold enough.

A sequence of polar orthographic plots (not shown) indicates that there is a buildup of HNO_3 inside the polar vortex in November, punctuated by meridional transport during the zonal wave- 1 events of early December and in January, and then followed by a splitting of the vortex in mid to late February. There is significant transport of HNO_3 from the polar region to middle equivalent latitudes (φ = 45 to 20˚) during those events. Meridional gradients of HNO_3 are larger in winter at both φ of 70˚ and near 20°, marking the polar and subtropical edges of the region of efficient meridional mixing. The subtropical boundary of the so-called "tropical pipe" region shifts from φ = 25˚ to about 15˚ from early December to late January and then remains at that location into springtime (Remsberg and Bhatt, 1996). There is erosion of the high HNO_3 values of the polar vortex by early March. Thereafter, HNO_3 decreases at all equivalent latitudes, due to the daily effects of the chemical re-partitioning of NO_y away from HNO_3 and toward NO and NO_2 ~~during sunlight~~under sunlit conditions.

Figure 14 displays the time series plot of the MLM for V6 H_2O, a better tracer of stratospheric transport. Relatively large values of 5.5 to 6.0 ppmv occur at high latitudes from mid-November to early January and indicate the effects of the slow descent of higher values within the vortex. H_2O is higher in the upper stratosphere from the oxidation of methane. Elevated H_2O values at φ > 75° on 13-15 and 19 January are due to residual emissions from PSCs. However, values of ~7 ppmv also appear in early February to mid-March, when temperatures are much too warm for the existence of PSCs. Although those higher values are within the uncertainties for retrieved H_2O, they compare well with times when there is ~~a~~ descent of higher ozone values in response to the major stratospheric warmings (c.f., Fig. 18 in Leovy et al., 1985).

Formatted: Left

Formatted: Normal

Finally, Figure 15 is the MLM plot of V6 NO_2 ~~is given in Figure 15~~, based on only its profiles along descending (nighttime) orbital segments. Smallest values of NO_2 occur in the polar vortex in late November and early December, when the HNO_3 values of Fig. 13 reach 13 ppbv. As with H_2O, there are several minor increases in NO_2 at the highest latitudes in mid-January~~:~~, and they occur at locations of residual effects from PSCs. The excess values of NO_2 poleward of $\varphi = 75^\circ$ in February occur where the variations of PV in Fig. 12 also indicate the effects of transport and where there may have been descent of higher NO_2 values within the vortex (Holt et al., 2012). The distribution of NO_2 away from the vortex varies more slowly and smoothly. Fig. 12 also indicates that there is considerable mixing for PV at $\varphi \sim$ 60° to 75° during February, and Fig. 15 shows that NO_2 is increasing along the PV contours. The vortex split into two sectors in the middle stratosphere from mid to late February, when there was transport and descent of air having higher NO_2 values at the high latitudes. NO_2 increases steadily from March to May, due to the conversion of HNO_3 to NO_2 upon the return of sunlight.

There are significant seasonal variations of NO_2 displayed in Fig. 15 at middle equivalent latitudes. ~~Conversion~~The re-partitioning of the NO_y species to HNO_3 occurs in the presence of background aerosols from late autumn to winter, followed by photochemical conversion of the HNO_3 vapor back to NO_2 in springtime (e.g., Austin et al., 1986). Fig. 15 shows that the very low values of NO_2 extend from near the Pole to at least $\varphi = 30^\circ$ in early December, and then ~~retreating~~retreat toward higher latitudes by late February. This variation of the NO_2 time series is an indicator of the so-called "Noxon cliff" feature of stratospheric column NO_2 during winter (e.g., Noxon, 1979). ~~Fig. 12 also indicates that there is considerable mixing for PV at φ ~ 60° to 75° during February, and Fig. 15 shows that NO_2 is increasing along the PV contours. The vortex split into two sectors in the middle stratosphere from mid to late~~

Formatted: Not Superscript/ Subscript

Formatted: Left

Formatted: Normal

~~February, when there was transport and descent of air having higher NO_x values at the high latitudes. NO_x increases steadily from March to May, due to the conversion of HNO_3 to NO_x upon the return of sunlight.~~

8 Conclusions

A significant improvement of the LIMS ~~V6~~ data set from V5 to V6 is the better accuracy of ~~its~~the retrieved V6 NO_2 profiles~~, particularly away from the cold winter vortex region~~. Both the V6 HNO_3 and NO_2 are of good quality, at least to within their respective error estimates and away from very cold regions of the vortex and their PSC remnants. ~~The~~The V6 species data are evaluated further in terms of the consistency of the HNO_3 and NO_2 distributions in the AH region during the minor warming event that took place in January 1979. In an earlier analysis of the LIMS V5 data, R93 highlighted an increase for HNO_3 at 30 hPa ~~in~~within the AH region ~~at 30 hPa~~ but with little change in NO_2~~within the AH region~~, and they suggested the need for some unknown process leading to the production of HNO_3 and to the development of the quasi-wave- 2 signature in its zonal distribution. ~~This~~The present study ~~considered~~considers photochemical model calculations along kinematic trajectories over a 10-day period that terminate in the AH region on 28 January. The results indicate that there was an increase of about 2 ppbv in HNO_3 and a decrease of order 0.5 ppbv in NO_2, mainly as a result of heterogeneous reactions converting N_2O_5 on surfaces of background stratospheric sulfuric acid aerosols. ~~R93~~R93 and Considine et al. (1992) alluded to this mechanism but reported that their ~~two and~~ three- and two-dimensional model studies with heterogeneous chemistry gave results that still did not agree well with the ~~observations from~~ LIMS V5~~. The~~ species. On the contrary, the latitudinal variations of HNO_3 at the end of our Lagrangian trajectory calculations agree reasonably with the LIMS V6 data. Those variations depend on the initial conditions and the extent of exposure of air parcels to sunlit and dark conditions, and hence on the

Formatted: Not Superscript/ Subscript

Formatted: Left

Formatted: Normal

dynamically controlled ~~history~~histories of the ~~different~~separate trajectories. Our model ~~results show~~calculations also reveal the formation of ~~the~~a dip in observed HNO_3 mixing ratios north of the AH, due to meridional transport of low latitude air across the Pole. Therefore, we conclude that the study approach of R93 was valid and should have led them to better comparisons, if the V6 data ~~were~~set had been available earlier.

~~The inclusion~~When the effects of heterogeneous ~~reactions improves~~chemistry are included in the model ~~comparisons for both~~calculations, the variations of HNO_3 and NO_2~~. The~~ along trajectories agree more reasonably with the LIMS V6 observations in the relatively isolated AH region. Yet, the model still underestimates NO_2 ~~for some trajectories~~ compared to the V6 values~~, however~~ along some trajectory paths. A part of those differences may be due to an inability to retrieve a local minimum in the V6 NO_2 profile with good accuracy, at least based on the finite, vertical field of view of the NO_2 channel radiances and their associated LIMS temperature profiles. Still, the present study demonstrates that a combination of dynamical and photochemical changes ~~will~~can explain the maximum mixing ratios of HNO_3 in both the AH region and at the winter polar vortex, ~~with~~plus its lower values around the periphery of both circulation systems. ~~When the effects of heterogeneous chemistry are included, the calculated variations of HNO_3 and NO_2 along trajectories agree more reasonably with the LIMS observations in the relatively isolated AH region.~~ HNO_3 re-partitions by photochemistry toward NO_2 ~~during~~from winter to springtime, when the anticyclone regions extend to middle latitudes. We also present examples of the seasonal evolution of HNO_3 and NO_2 during 1978-1979 as a separate aspect of the V6 data set for the validation of chemistry/climate models ~~in~~of the middle to lower stratosphere.

Formatted: Font color: Black

Formatted: Font color: Black

Formatted: Font color: Black

Formatted: Left

Formatted: Normal

582 **Acknowledgements.** The LIMS V6 data set is archived at the Goddard Earth Sciences Data and
583 Information Services Center (GES DISC and its Website: daac.gsfc.nasa.gov) and is accessible for
584 scientific use via ftp download.

585

Formatted: Left

Formatted: Normal

References

Austin, J. A., Garcia, R. R., Russell III, J. M., Solomon, S., and Tuck, A. F.: On the atmospheric photochemistry of nitric acid, J. Geophys. Res., 91, 5477-5485, 1986.

Baldwin, M. P., and Holton, J. R.: Climatology of the stratospheric polar vortex and planetary wave breaking, J. Atmos. Sci., 45, 1123-1142, 1988.

Brasseur, G. P. and Solomon, S.: Aeronomy of the middle atmosphere, 3rd Edition, Springer, The Netherlands, 644 pp., 2005.

Burkholder, J. B., Sander, S. P., Abbatt, J., Barker, J. R., Huie, R. E., Kolb, C. E., Kurylo, M. J., Orkin, V. L., Wilmouth, D. M., and Wine, P. H.: Chemical kinetics and photochemical data for use in atmospheric studies, Evaluation No. 18, JPL Publication 15-10, Jet Propulsion Laboratory, Pasadena, 2015, http://jpldataeval.jpl.nasa.gov.

Butchart, N. and Remsberg, E. E.: The area of the stratospheric polar vortex as a diagnostic for tracer transport on an isentropic surface, J. Atmos. Sci., 43, 1319-1339, 1986.

Callis, L. B., Natarajan, M., Lambeth, J. D., and Boughner, R. E.: On the Origin of Midlatitude Ozone Changes: Data Analysis and Simulations for 1979 -1993, J. Geophys. Res., 102, 1215-1228, 1997.

Formatted: Left

Formatted: Normal

Colucci, S. J., and Ehrmann, T. S.: Synoptic-dynamic climatology of the Aleutian High, J. Atmos. Sci., 75, 1271-1283, doi:10.1175/JAS-D-17-0215.1, 2018.

Considine, D. B., Douglass, A. R., and Stolarski, R. S.: Heterogeneous conversion of N_2O_5 to HNO_3 on background stratospheric aerosols: comparisons of model results with data, Geophys. Res. Lett., 19, 397-400, 1992.

Eyring, V., Lamarque, J.-F., Hess, P., Arfeuille, F., Bowman, K., Chipperfield, M. P., Duncan, B., Fiore, A., Gettelman, A., Giorgetta, M. A., Granier, C., Hegglin, M., Kinnison, D., Kunze, M., Langematz, U., Luo, B., Martin, R., Matthes, K., Newman, P. A., Peter, T., Robock, A., Ryerson, T., Saiz-Lopez, A., Salawitch, R., Schultz, M., Shepherd, T. G., Shindell, D., Staehelin, J., Tegtmeier, S., Thomason, L., Tilmes, S., Vernier, J.-P., Waugh, D. W., and Young, P. J.: Overview of IGAC/SPARC chemistry-climate model initiative (CCMI) community simulations in support of upcoming ozone and climate assessments, SPARC Newsletter No. 40, January, 2013.

Gille, J. C. and Russell III, J. M.: The limb infrared monitor of the stratosphere: experiment description, performance, and results, J. Geophys. Res., 89, 5125-5140, 1984.

Harvey, V. L. and Hitchman, M. H.: A climatology of the Aleutian High, J. Atmos. Sci., 53, 2088-2101, 1996.

Formatted: Left

Formatted: Normal

Harvey, V. L., Pierce, R. B., Hitchman, M. H., Randall, C. E., and Fairlie, T. D.: On the distribution of ozone in stratospheric anticyclones, J. Geophys. Res., 109, D24308, doi:10.1029/2004JD004992, 2004.

Harvey, V. L., Randall, C. E., and Hitchman, M. H.: Breakdown of potential vorticity-based equivalent latitude as a vortex-centered coordinate in the polar winter mesosphere, J. Geophys. Res., 114, D22105, doi:10.1029/2009JD012681, 2009.

Hofmann, D. J., and Solomon, S.: Ozone destruction through heterogeneous chemistry following the eruption of El Chichon, J. Geophys. Res., 94, D4, 5029-5041, 88JD04231, 1989.

Holt, L. A., Randall, C. E., Harvey, V. L., Remsberg, E. E., Stiller, G. P., Funke, B., Bernath, P. F., and Walker, K. A.: Atmospheric effects of energetic particle precipitation in the Arctic winter 1978-1979 revisited, J. Geophys. Res., 117, D05315, doi:10.1029/2011JD016663, 2012.

Juckes, M. N., and McIntyre, M. E.: A high-resolution one-layer model of breading planetary waves in the stratosphere, Nature, 328, 590-596, 1987.

Juckes, M. N., and O'Neill, A.: Early winter in the northern stratosphere, Quart. J. R. Meteorol. Soc., 114, 1111-1125, 10.1002/qj.49711448211, 1988.

Formatted: Left

Formatted: Normal

Lambert, A., Santee, M. L., Wu, D. L., and Chae, J. H.: A-train CALIOP and MLS observations of early winter Antarctic polar stratospheric clouds and nitric acid in 2008, Atmos. Chem. Phys., 12, 2899-2931, doi:10.5194/acp-12-2899-2012, 2012.

Leovy, C. B., Sun, C.R., Hitchman, M. H., Remsberg, E. E., Russell III, J. M., Gordley, L. L., Gille, J. C., and Lyjak, L. V.: Transport of ozone in the middle stratosphere: evidence for planetary wave breaking, J. Atmos. Sci., 42, 230-244, 1985.

Manney, G. L., Froidevaux, L., Waters, J. W., Zurek, R. W., Gille, J. C., Kumer, J. B., Mergenthaler, J. L., Roche, A. E., O'Neill, A., and Swinbank, R.: Formation of low-ozone pockets in the middle stratospheric anticyclone during winter, J. Geophys. Res., 100, D7, 13,939-13,950, 1995.

McIntyre, M. E.: Towards a Lagrangian-mean description of stratospheric circulations and chemical transport, Phil. Trans. R. Soc. London, A296, 129-148, 1980.

McIntyre, M. E.: The stratospheric polar vortex and sub-vortex: fluid dynamics and midlatitude ozone loss, Phil. Trans. R. Soc. London, A352, 227-240, 1995.

McIntyre, M. E. and Palmer, T. N.: Breaking planetary waves in the stratosphere, Nature, 305, 593-600, 1983.

Formatted: Left

Formatted: Normal

Morris, G. A., Kawa, S. R., Douglass, A. R., Schoeberl, M. R., Froidevaux, L., and Waters, J.: Low-ozone pockets explained, J. Geophys. Res., 103, D3, 3599-3610, 1998.

Natarajan, M. and Callis, L. B.: Stratospheric photochemical studies with Atmospheric Trace Molecule Spectroscopy (ATMOS) measurements, J. Geophys. Res., 96, D5, 9361-9370, doi:10.1029/91JD00290, 1991.

Natarajan, M. and Callis, L. B.: Ozone variability in the high latitude summer stratosphere, Geophys. Res. Lett., 24, no. 10, 1191-1194, 1997.

Natarajan, M., Remsberg, E. E., and Gordley, L. L.: Ozone budget in the upper stratosphere: model studies using the reprocessed LIMS and the HALOE datasets, Geophys. Res. Lett., 29, no. 7, doi:10.1029/2001GL014262, 2002.

Noxon, J.: Stratospheric NO_2, 2. global behavior, J. Geophys. Res., 84, no. C8, 5067-5076, 1979.

Remsberg, E. E., and Bhatt, P. P.: Zonal variance of nitric acid vapor as an indicator of meridional mixing in the subtropical lower stratosphere, J. Geophys. Res., 101, 29,523-29,530, 1996.

Remsberg, E. and Harvey, V. L.: Effects of polar stratospheric clouds in the Nimbus 7 LIMS Version 6 data set, Atmos. Meas. Tech., 9, 2927-2946, doi:10.5194/amt-9-2927-2016, 2016.

Formatted: Left

Formatted: Normal

Remsberg, E. and Lingenfelser, G.: LIMS Version 6 Level 3 dataset, NASA/TM-2010-216690, available at http://www.sti.nasa.gov (last access: 6 May 2015), 13 pp., 2010.

Remsberg, E. E., Bhatt, P. P., Eckman, R. S., Gordley, L. L., Russell III, J. M., and Siskind, D. E.: Effect of the HITRAN 92 spectral data on the retrieval of NO_2 mixing ratios from Nimbus 7 LIMS, J. Geophys. Res., 99, D11, 22,965-22,973, 94JD02042, 1994.

Remsberg, E. E., Gordley, L. L., Marshall, B. T., Thompson, R. E., Burton, J., Bhatt, P., Harvey, L. V., Lingenfelser, G., and Natarajan, M.: The Nimbus 7 LIMS version 6 radiance conditioning and temperature retrieval methods and results, J. Quant. Spectros. Rad. Transf., 86, 395-424, doi:10.1016/j.jqsrt.2003.12.007, 2004.

Remsberg, E., Lingenfelser, G., Natarajan, M., Gordley, L., Marshall, B. T., and Thompson, E.: On the quality of the Nimbus 7 LIMS version 6 ozone for studies of the middle atmosphere, J. Quant. Spectros. Rad. Transf., 105, 492-518, doi:10.1016/j.jqsrt.2006.12.005, 2007.

Remsberg, E. E., Natarajan, M., Lingenfelser, G. S., Thompson, R. E., Marshall, B. T., and Gordley, L. L.: On the quality of the Nimbus 7 LIMS Version 6 water vapor profiles and distributions, Atmos. Chem. Phys., 9, 9155-9167, https://doi.org/10.5194/acp-9-9155-2009, 2009.

Formatted: Left

Formatted: Normal

718 Remsberg, E., Natarajan, M., Marshall, B. T., Gordley, L. L., Thompson, R. E., and
719 Lingenfelser, G.: Improvements in the profiles and distributions of nitric acid and nitrogen
720 dioxide with the LIMS version 6 dataset, Atmos. Chem. Phys., 10, 4741-4756, doi:10.5194/acp-
721 10-4741-2010, 2010.
722
723 Remsberg, E., Natarajan, M., Fairlie, T. D., Wargan, K., Pawson, S., Coy, L., Lingenfelser, G.,
724 and Kim, G.: On the inclusion of Limb Infrared Monitor of the Stratosphere version 6 ozone in a
725 data assimilation system, J. Geophys. Res., 118, 7982-8000, doi:10.1002/jgrd.50566, 2013.
726
727 Rienecker, M.M., Suarez, M. J., Gelaro, R., Todling, R., Bacmeister, J., Liu, E., Bosilovich, M.
728 G., Schubert, S. D., Takacs, L., Kim, G.-K., Bloom, S., Chen, J., Collins, D., Conaty, A., da
729 Silva, A., Wei G., Joiner, J. , Koster R. D., Lucchesi, R., Molod, A., Owens, T., Pawson, S.,
730 Pegion, P., Redder, C. R., Reichle, R., Robertson, F. R., Ruddick, A. G., Sienkiewicz, M., and
731 Woollen, J.: MERRA: NASA's Modern-Era Retrospective Analysis for Research and
732 Applications. J. Climate, 24, 3624-3648, doi:10.1175/JCLI-D-11-00015.1, 2011.
733
734 Rodriguez, J. M., Ko, M. K. W., and Sze, N. D.: Role of heterogeneous conversion of N_2O_5 on
735 sulfate aerosols in global ozone losses, Nature, 352, 134-137, doi:10.1038/352134a0, 1991.
736
737 Rood, R. B., Kaye, J. A., Nielsen, J. E., Schoeberl, M. R., and Geller, M. A.: Nitric acid forecast
738 experiments, Physica Scripta, 36, 337-354, 1987.
739

Formatted: Left

Formatted: Normal

740 Rood, R. B., Douglass, A. R., Kaye, J. A., and Considine, D. B.: Characteristics of wintertime
741 and autumn nitric acid chemistry as defined by limb infrared monitor of the stratosphere (LIMS)
742 data, J. Geophys. Res., 98, 18,533-18,545, 1993.
743
744 Rose, K.: The stratospheric winter polar vortex simulated as a material entity, J. Atmos. Terr.
745 Phys., 48, 1197-1202, 1986.
746
747 SPARC: The SPARC Data Initiative: Assessment of stratospheric trace gas and aerosol
748 climatologies from satellite limb sounders. M. I. Hegglin and S. Tegtmeier (Eds.), SPARC
749 Report No. 8, WCRP-05/2017, doi:10.3929/ethz-a-010863911, available at www.sparc-
750 climate.org/publications/sparc-reports/, 2017.
751
752 Shepherd, T. G., Plummer, D. A., Scinocca, J. F., Hegglin, M. I., Fioletov, V. E., Reader, M. C.,
753 Remsberg, E., von Clarmann, T., and Wang, H. J.: Reconcilation of halogen-induced ozone loss
754 with the total-column ozone record, Nature Geoscience, 7, 443–449, doi:10.1038/ngeo2155,
755 2014.
756
757 Stolarski, R. S., Douglass, A. R., Remsberg, E. E., Livesey, N. J., and Gille, J. C.: Ozone
758 temperature correlations in the upper stratosphere as a measure of chlorine content, J. Geophys.
759 Res., 117, D10305, doi:10.1029/2012JD017456, 2012.
760

Formatted: Left

Formatted: Normal

761 Tegtmeier, S., Hegglin, M. I., Anderson, J., Bourassa, A., Brohede, S., Degenstein, D.,
762 Froidevaux, L., Fuller, R., Funke, B., Gille, J., Jones, A., Kasai, Y., Krüger, K., Kyrölä, E.,
763 Lingenfelser, G., Lumpe, J., Nardi, B., Neu, J., Pendlebury, D., Remsberg, E., Rozanov, A.,
764 Smith, L., Toohey, M., Urban, J., von Clarmann, T., Walker, K. A., Wang, R. H. J.: SPARC
765 Data Initiative: A comparison of ozone climatologies from international satellite limb sounders,
766 J. Geophys. Res., 118, 12,229–12,247, doi:10.1002/2013JD019877, 2013.
767

Formatted: Left

Formatted: Normal

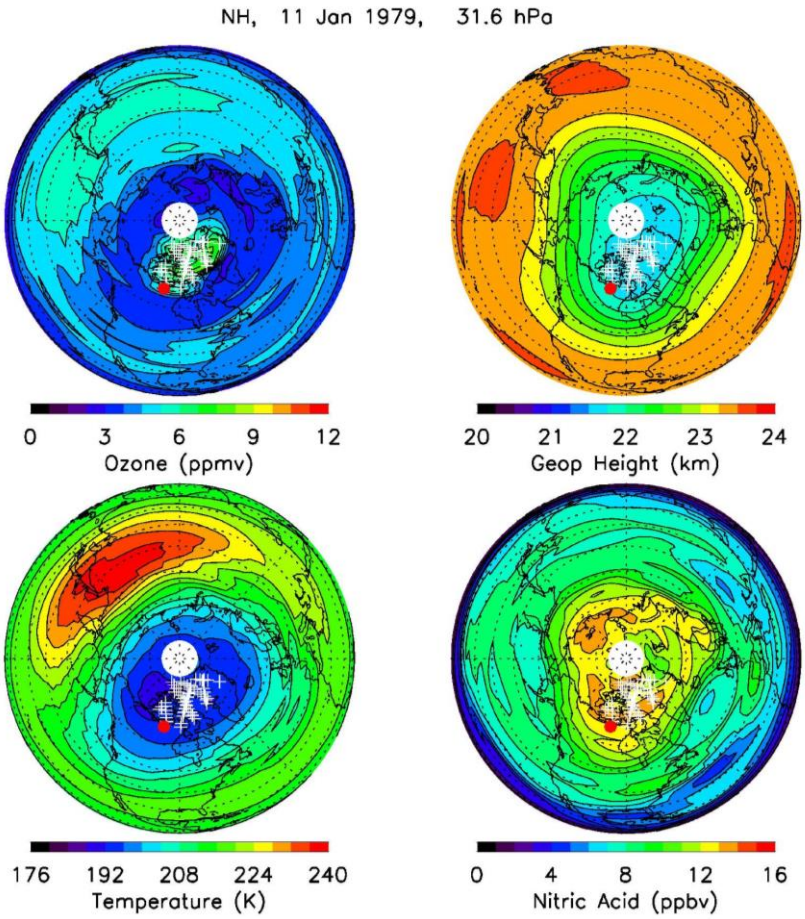

Von König, M., Bremer, H., Kleinböhl, A., Küllmann, H., Künzi, K. F., Goede, A. P. H., Browell, E. V., Grant, W. B., Burris, J. F., McGee, T. J., and Twigg, L.: Using gas-phase nitric

Formatted: Left

Formatted: Normal

773 acid as an indicator of PSC composition, J. Geophys. Res., 107, D20, 8265,
774 doi:10.1029/2001JD001041, 2002.
775

Formatted: Left
Formatted: Normal

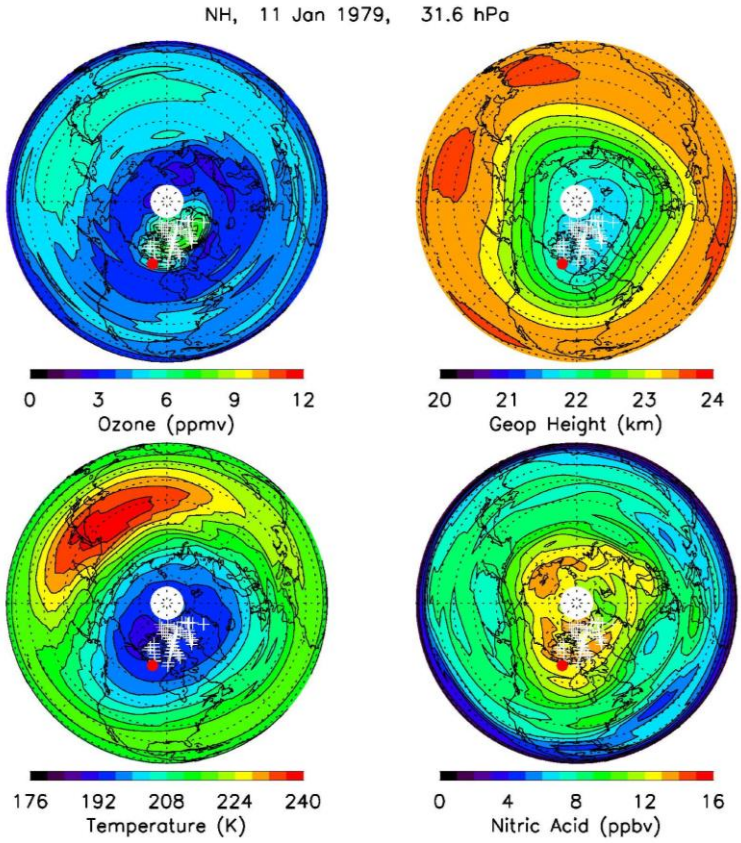

Figure 1. Polar orthographic projections of Northern Hemisphere ozone (top left), geopotential height (GPH, top right), temperature (bottom left), and gas phase nitric acid (bottom right) for 11 January 1979 at 31.6 hPa; successive latitude circles are at every 10˚. The Greenwich meridian extends horizontally to the right. Contour intervals are every 0.75 ppmv for ozone, 0.25 km for GPH, 4 K for temperature, and 1 ppbv for nitric acid. White plus signs denote orbital profile segments that are missing; red dot denotes location of a SAM II PSC observation.

Formatted: Left

Formatted: Normal

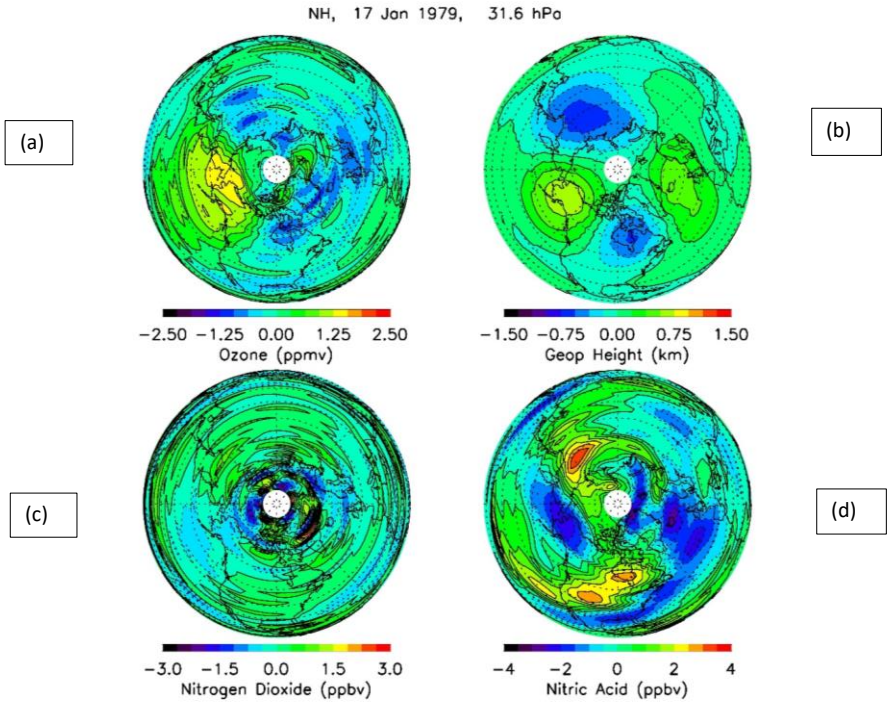

Figure 2. Zonal anomalies of ozone, GPH, nitrogen dioxide, and nitric acid for 31.6 hPa on 17 January 1979.

Formatted: Left

Formatted: Normal

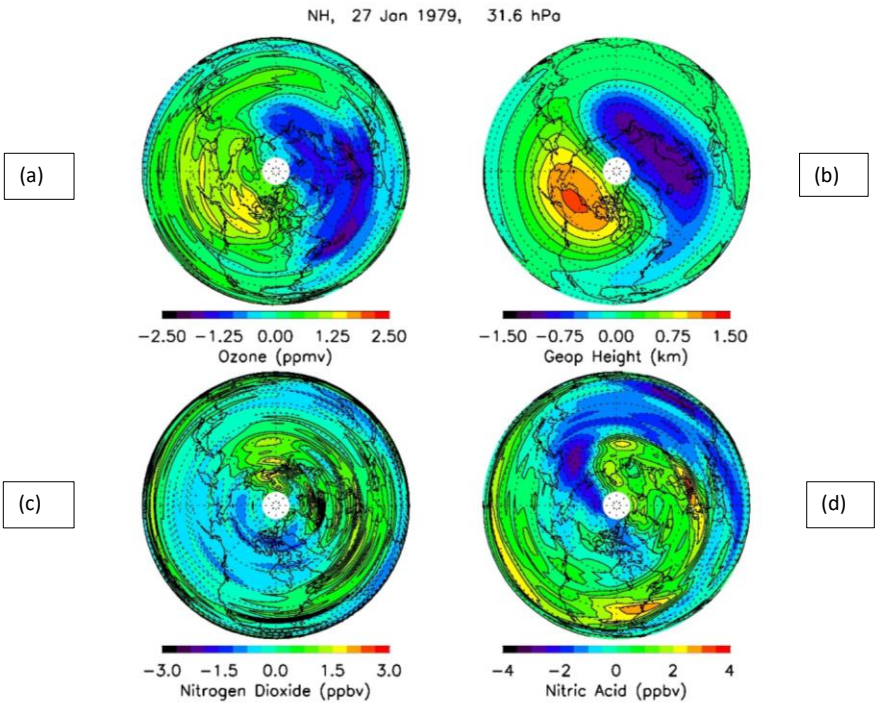

Figure 3. As in Fig. 2, but for 27 January 1979.

Formatted: Left

Formatted: Normal

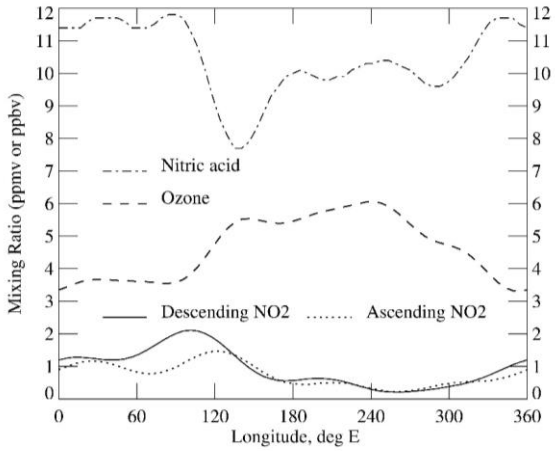

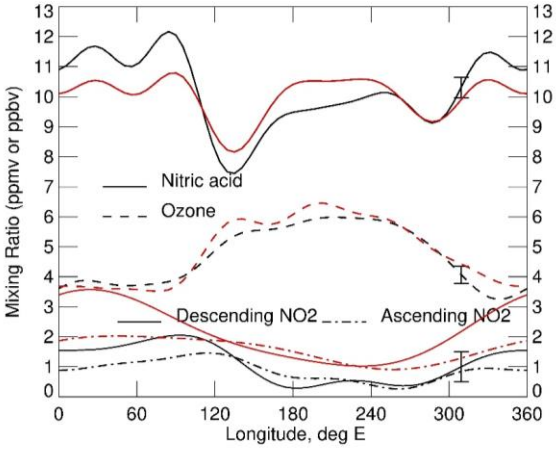

Figure 4. Zonal variations of LIMS V6 (black) and V5 (red) species at ~~66°~~64° N on 27 January 1979. Vortex is between 0 and 90° E, and AH region is from 180 and 240° E. Vertical bars on

Formatted: Left

Formatted: Normal

curves near 311°E are 2σ estimates of the error. Ozone has units of ppmv, while HNO_3 and NO_2 (its separate descending and ascending curves at bottom) have units of ppbv.

Formatted: Left

Formatted: Normal

804

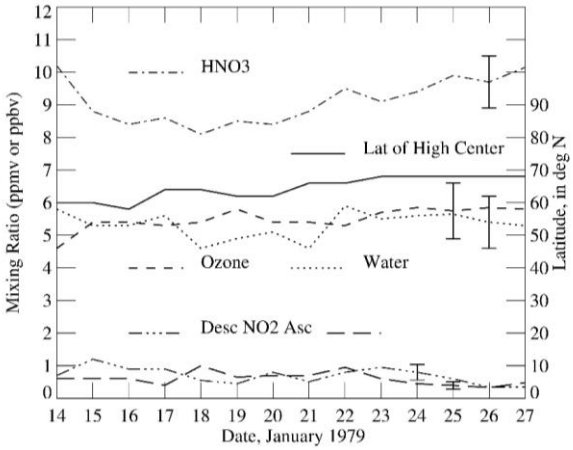

805

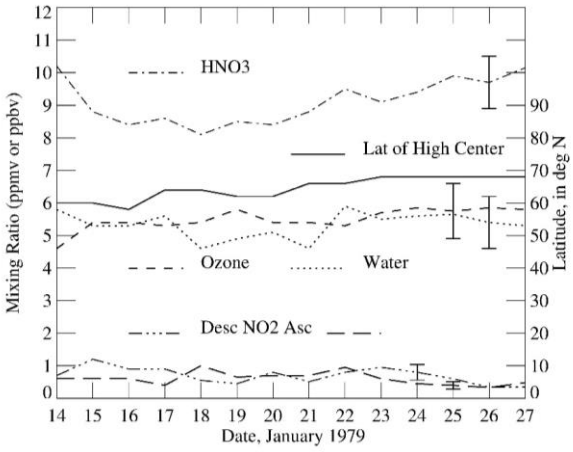

806

807 **Figure 5.** Time series of observed LIMS V6 species at 31.6 hPa and ~~at the center of~~ the Aleutian
808 High (AH) anomaly; ~~its~~ latitude of AH center is the solid curve. The species curves have vertical

Formatted: Left

Formatted: Normal

bars ~~from~~near 24 to 26 January ~~that indicate~~indicating their ±RSS errors. Ozone and water have units of ppmv, while NO_2 and HNO_3 have units of ppbv.

Formatted: Left

Formatted: Normal

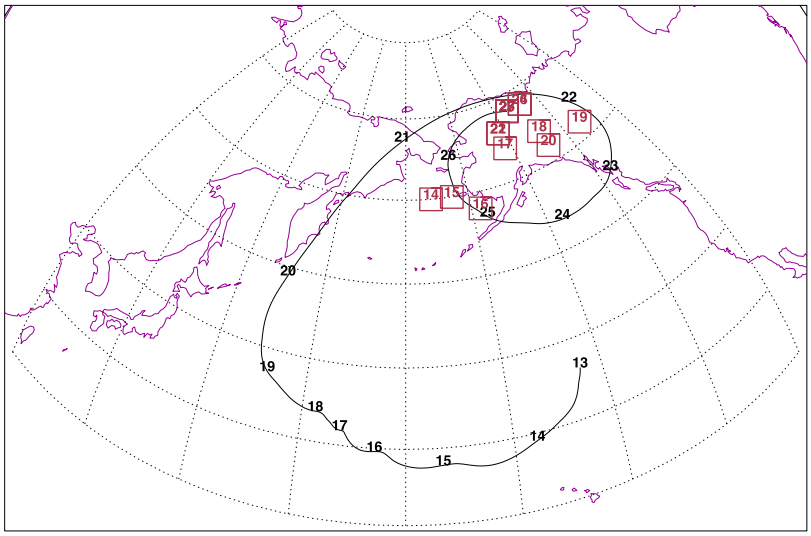

Figure 6. History of the location of maximum GPH anomaly at 31.6 hPa representing the AH center and displayed by red squares with day numbers. Latitude spacing is 10° beginning at 20° N and longitude spacing is 15° beginning at 120° E. Note that between 21 and 27 January there is some repetition of the AH center ~~occupies~~locations, and the ~~same location on different days~~corresponding red squares overlap. The location on 27 January is 214° E and 68°N. Black line with day numbers describes the back trajectory beginning at 214° E, 68° N, and 30 hPa.

Formatted: Left

Formatted: Normal

821

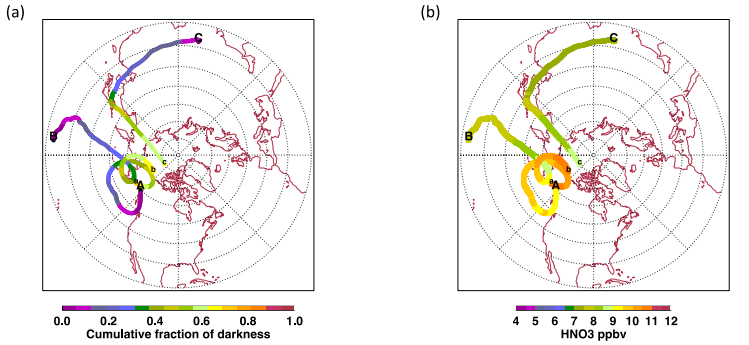

822

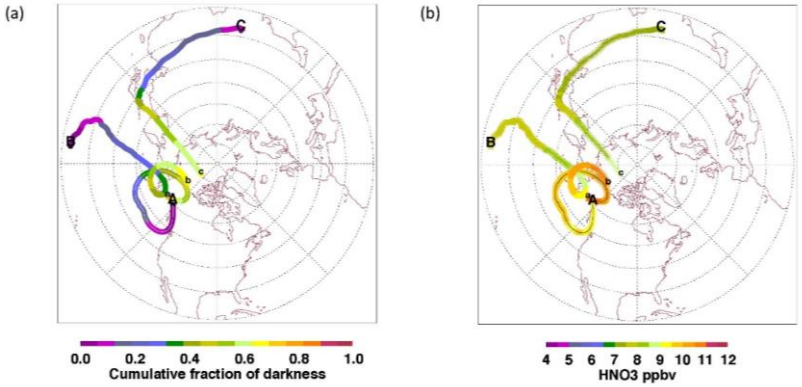

823

824

Formatted: Left

Formatted: Normal

Figure 7. (a) Back trajectories beginning at 11~~:00~~ pm on 27 January (9Z on January 28) from 30 hPa, 214° E, and three different latitudes **[a]** 60° N, **[b]** 72° N, and **[c]** 80° N. The corresponding endpoints **A, B**, and **C** are spatially and temporally closest to LIMS descending mode measurement locations between 14 and 17 January. The latitude grids are 10° apart, starting from 20° N and the Prime meridian extends horizontally to the right. The color scale refers to the accumulated hours of darkness expressed as a fraction of the total length of the trajectory in hours as the air parcel moves in the forward direction starting from locations **A, B,** and **C** and ending at **a, b,** or **c** along 214° E longitude. (b) Evolution of HNO_3 along the three trajectories that were shown in ~~the left panel.~~(a).

Formatted: Left

Formatted: Normal

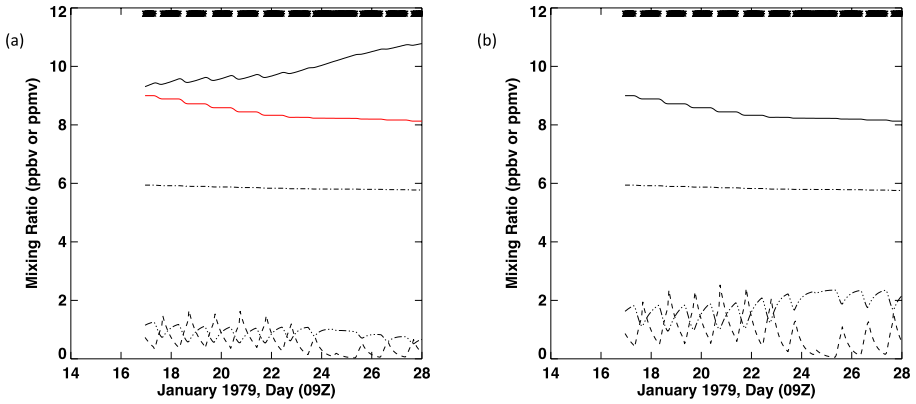

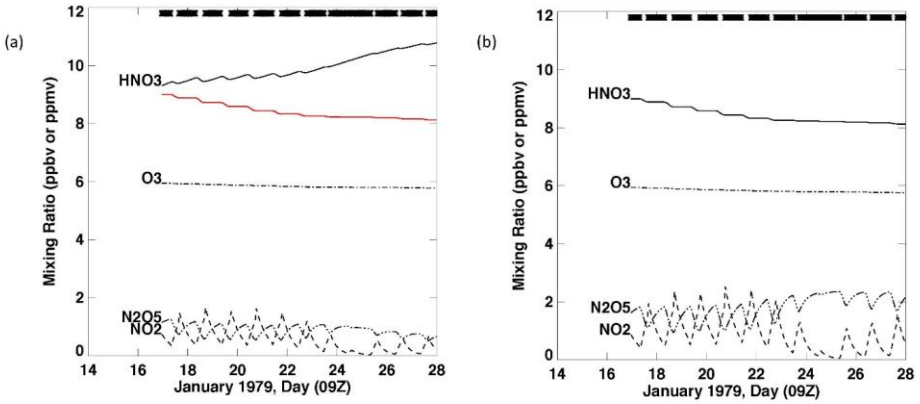

Formatted: Left

Formatted: Normal

Figure 8. Mixing ratio of selected species as a function of time along the trajectory A-a shown in Figure 7a. Air parcel terminates at 214° E and 60° N. HNO_3 (solid), NO_2 (dash), and N_2O_5 (dash-dot-dot) are in ppbv, and ozone (dash-dot) is in ppmv. The tick marks on the abscissa correspond to 09Z hours on the dates shown. The thick line at the top represents the periods of darkness along the trajectory with intermittent gaps corresponding to sunlit segments. (a) Results from the case including heterogeneous reactions~~. (b) Results from the case with only~~, but with the red curve showing HNO_3 from only the gas phase chemistry for comparison; (b) Results for all species from only the gas phase reactions.

Formatted: Left

Formatted: Normal

848

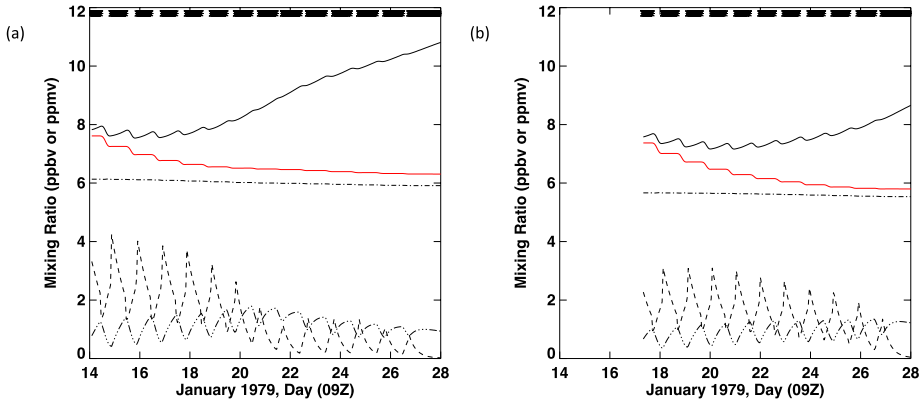

849

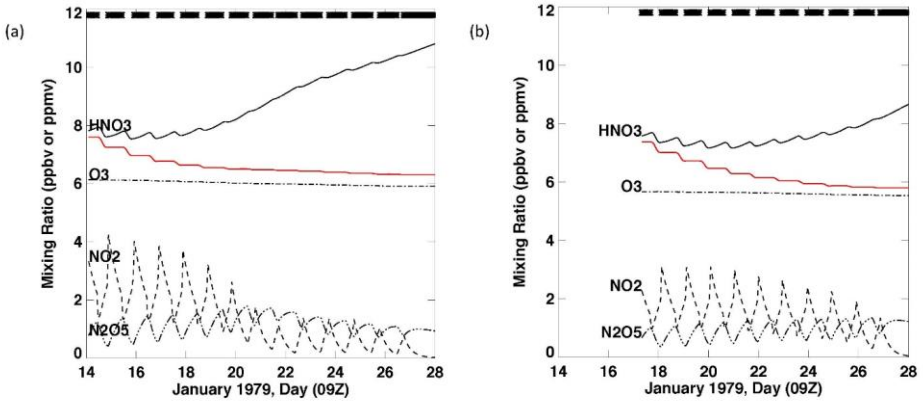

850

851

Formatted: Left

Formatted: Normal

852 **Figure 9.** Mixing ratio of selected species as a function of time for the case with heterogeneous
853 reactions as shown in Figure 8a but for trajectory B-b (a) and trajectory C-c (b). HNO_3 (solid),
854 NO_2 (dash), and N_2O_5 (dash-dot-dot) are in ppbv, and ozone (dash-dot) is in ppmv. The red
855 ~~line~~curve in both panels represent the HNO_3 variation for the case with only gas phase reactions.
856

Formatted: Left

Formatted: Normal

857

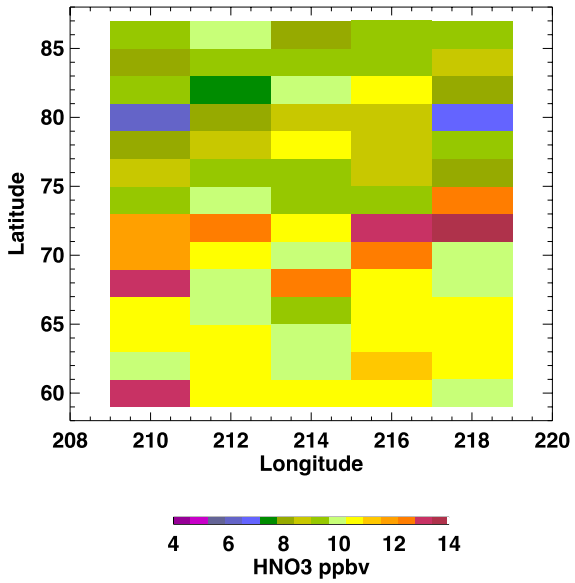

858

859

860 **Figure 10.** Calculated HNO_3 at 09Z on 28 January, corresponding to terminal location of all 70
861 trajectories.

862

Formatted: Left

Formatted: Normal

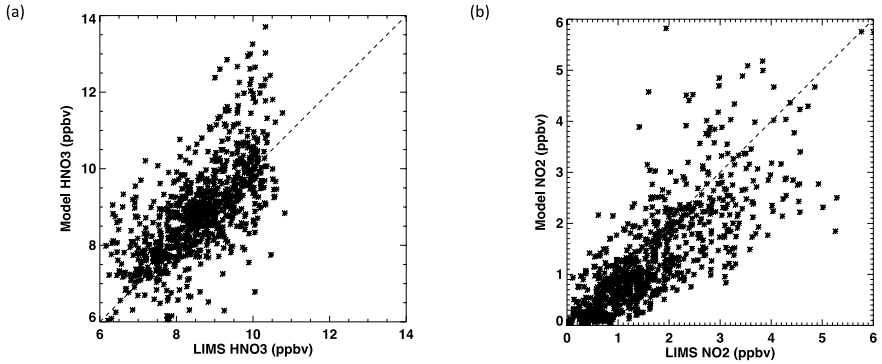

Figure 11. Scatter plot of calculated species mixing ratios along the 70 trajectories and of the corresponding spatially and temporally closest LIMS V6 observation. (a) HNO_3; (b) NO_2.

Formatted: Left

Formatted: Normal

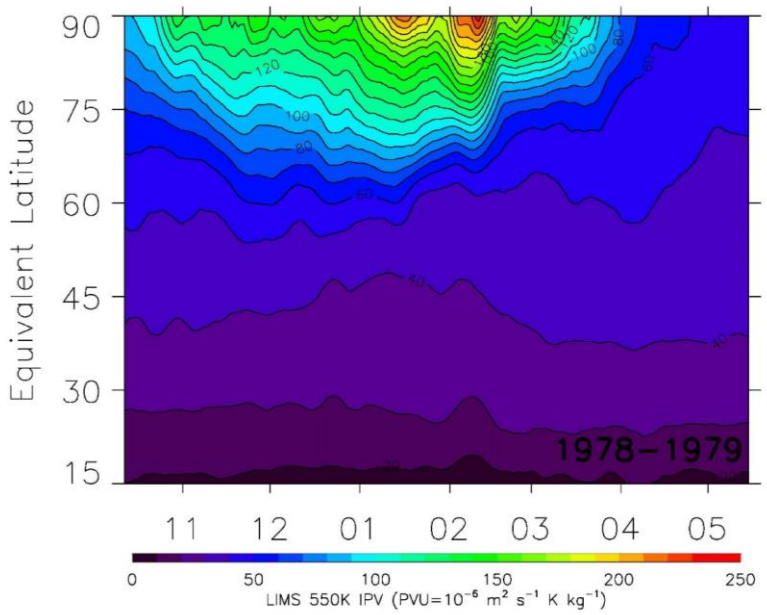

870

Formatted: Left

Formatted: Normal

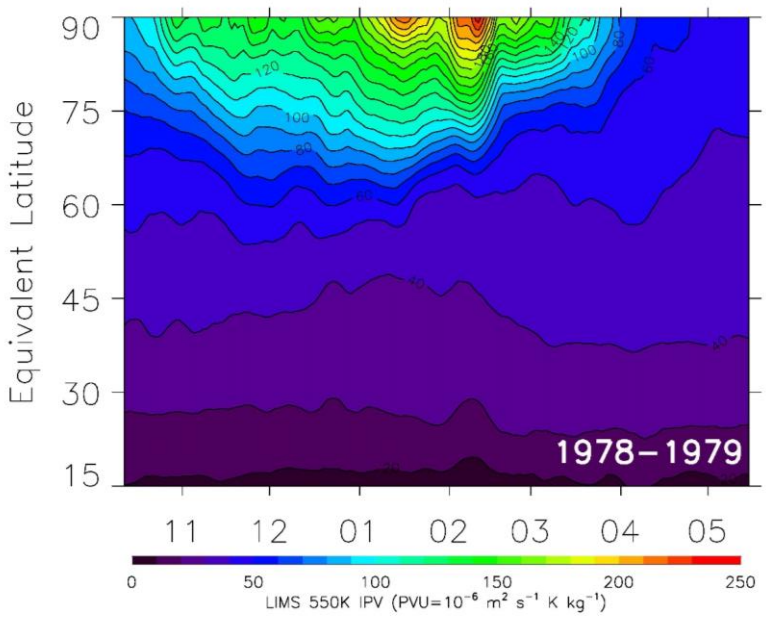

Figure 12. Time series of LIMS isentropic PV versus equivalent latitude at 550 K and with smoothing over 7 days. PV contour interval (CI) is 10 units.

Formatted: Left

Formatted: Normal

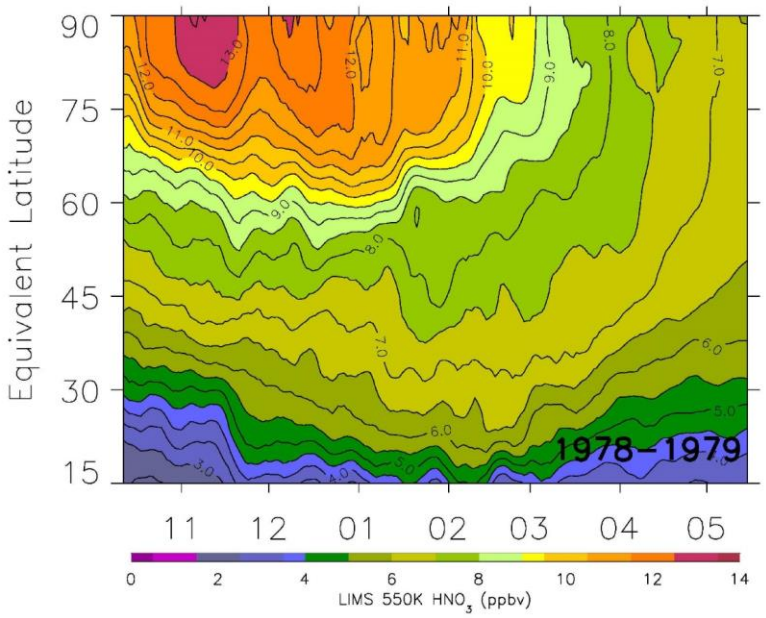

876

877 **Figure 13.** As in Fig. 12, but the averages of HNO_3 along PV isolines (CI is 0.5 ppbv).

878

879

Formatted: Left

Formatted: Normal

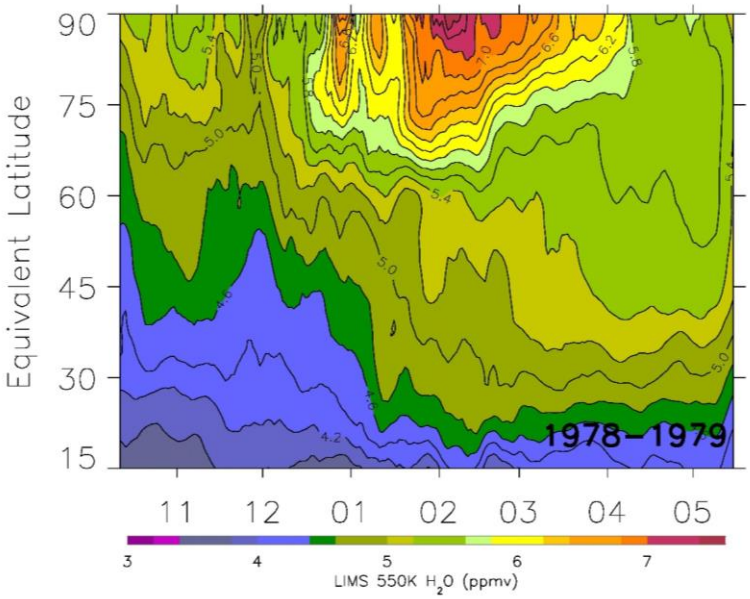

880

881 **Figure 14**. As in Fig. 13, but as averages of H_2O (CI = 0.2 ppmv).

882

883

Formatted: Left

Formatted: Normal

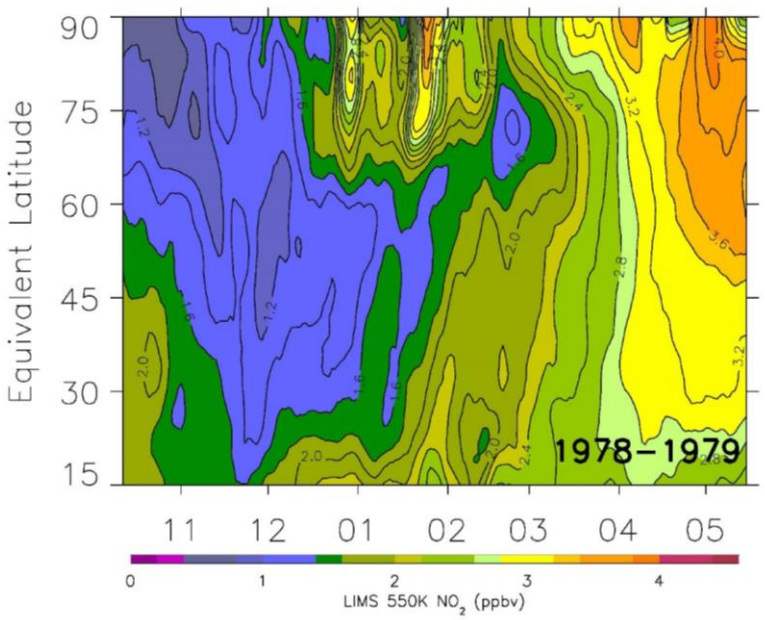

884

885 **Figure 15.** As in Fig. 13, but as averages of descending orbital (nighttime) NO_2 (CI = 0.2 ppbv).

886

Formatted: Left

Formatted: Normal